Article

TRANSPARENT PROCESS

EMBO reports

HDAC inhibitors tune miRNAs in extracellular vesicles of dystrophic muscle-resident mesenchymal cells

Martina Sandonà[1,2,†], Silvia Consalvi[1,†], Luca Tucciarone[1,2], Marco De Bardi[1], Manuel Scimeca[3,4,5], Daniela Francesca Angelini[1], Valentina Buffa[6], Adele D'Amico[7], Enrico Silvio Bertini[7], Sara Cazzaniga[8], Paolo Bettica[8], Marina Bouché[2], Antonella Bongiovanni[6], Pier Lorenzo Puri[9,*] & Valentina Saccone[1,10,**]

Abstract

We show that extracellular vesicles (EVs) released by mesenchymal cells (i.e., fibro–adipogenic progenitors—FAPs) mediate microRNA (miR) transfer to muscle stem cells (MuSCs) and that exposure of dystrophic FAPs to HDAC inhibitors (HDACis) increases the intra-EV levels of a subset of miRs, which cooperatively target biological processes of therapeutic interest, including regeneration, fibrosis, and inflammation. Increased levels of miR-206 in EVs released by FAPs of muscles from Duchenne muscular dystrophy (DMD) patients or mdx mice exposed to HDACi are associated with enhanced regeneration and decreased fibrosis. Consistently, EVs from HDACi-treated dystrophic FAPs can stimulate MuSC activation and expansion *ex vivo*, and promote regeneration, while inhibiting fibrosis and inflammation of dystrophic muscles, upon intramuscular transplantation in mdx mice, *in vivo*. AntagomiR-mediated blockade of individual miRs reveals a specific requirement of miR-206 for EV-induced expansion of MuSCs and regeneration of dystrophic muscles, and indicates that cooperative activity of HDACi-induced miRs accounts for the net biological effect of these EVs. These data point to pharmacological modulation of EV content as novel strategy for therapeutic interventions in muscular dystrophies.

Keywords duchenne muscular dystrophy; extracellular vesicles; HDAC inhibitors; microRNA; muscle regeneration

Subject Categories Molecular Biology of Disease; RNA Biology; Stem Cells & Regenerative Medicine

DOI 10.15252/embr.202050863 | Received 11 May 2020 | Revised 1 July 2020 | Accepted 6 July 2020

EMBO Reports (2020) e50863

Introduction

Emerging evidence indicates that reciprocal interactions between distinct cellular components of the regeneration "machinery" generate either a productive or a hostile environment for regeneration of dystrophic muscles (Moyer & Wagner, 2011; Tidball, 2011; Farup *et al*, 2015). While muscle stem (satellite) cells (Mauro, 1961) (therein indicated as MuSCs) are the direct effectors of muscle repair, a variety of other cell types contribute to muscle regeneration, by spatially and temporally coordinating the activity of MuSCs (Bentzinger *et al*, 2013; Dumont *et al*, 2015b). These cells comprise components of the inflammatory infiltrate, including macrophages and eosinophils (Kharraz *et al*, 2013; Tidball *et al*, 2014), and a heterogeneous population of muscle-derived interstitial cells referred to as fibro–adipogenic progenitors (FAPs) (Joe *et al*, 2010; Uezumi *et al*, 2010; Malecova *et al*, 2018). Disruption of this network compromises the integrity of MuSC niche and has been associated with the progression of many chronic muscular disorders (i.e., muscular dystrophies) and age-related decline in muscle mass and repair (Uezumi *et al*, 2011; Blau *et al*, 2015).

Upon myofiber damage, FAP accumulation is preceded by the appearance of the inflammatory infiltrate and is followed by MuSC activation (Heredia *et al*, 2013; Lemos *et al*, 2015). This temporal

1 Istituto di Ricovero e Cura a Carattere Scientifico (IRCCS), Fondazione Santa Lucia, Rome, Italy
2 Division DAHFMO, Unit of Histology and Medical Embryology, Sapienza University of Rome, Rome, Italy
3 Department of Biomedicine and Prevention, University of Rome "Tor Vergata", Rome, Italy
4 IRCCS San Raffaele Pisana, Rome, Italy
5 Orchidea Lab S.r.l., Rome, Italy
6 Institute of Biomedicine and Molecular Immunology (IBIM), National Research Council (CNR) of Italy, Palermo, Italy
7 Unit of Neuromuscular and Neurodegenerative Disorders, Bambino Gesù Children's Hospital, Rome, Italy
8 Clinical R&D Italfarmaco SpA, Cinisello Balsamo, Italy
9 Development, Aging and Regeneration Program, Sanford Burnham Prebys Medical Discovery Institute, La Jolla, CA, USA
10 Dipartimento Scienze della Vita e Sanità Pubblica, Università Cattolica del Sacro Cuore, Rome, Italy
*Corresponding author. Tel: +1 (858) 646-3100; E-mail: lpuri@sbpdiscovery.org
**Corresponding author. Tel: +39 (06) 501703266; E-mail: v.saccone@hsantalucia.it
†These authors contributed equally to this work

pattern suggests a key role for FAPs in converting inflammatory cues into signals that regulate MuSC activity, and implies reciprocal communications between these cell types, through the exchange of soluble mediators, which are largely unknown. Deciphering the molecular and functional identity of these mediators might reveal selective targets for interventions aimed at restoring functional interactions between cellular components of the skeletal muscle environment during maladaptive repair in chronic muscular disorders.

Previous studies identified FAPs as key cellular targets of histone deacetylase inhibitor (HDACi)—a pharmacological intervention that counters DMD progression by promoting compensatory regeneration, while inhibiting fibro–adipogenic degeneration both in pre-clinical studies (Minetti *et al*, 2006; Consalvi *et al*, 2011, 2013, 2016; Mozzetta *et al*, 2013; Saccone *et al*, 2014; Sandoná *et al*, 2016) and in clinical trials (Bettica *et al*, 2016). While these studies indicate the pharmacological potential of HDACi to restore the regenerative environment in dystrophic muscles, by recovering physiological functional interactions between FAPs and other cellular components (Consalvi *et al*, 2014), the signals that mediate HDACi ability to restore physiological interactions between FAPs and other cell types in DMD muscles remain largely unknown.

Here, we report the identification and functional characterization of extracellular vesicles (EVs) that mediate FAP's ability to promote MuSC activation and differentiation, as well as to inhibit muscle fibrosis and inflammation, in DMD muscles exposed to HDACi, through the cooperative activities of miR-206 and other HDACi-induced intra-EV miRs.

Results

EVs mediate FAP ability to promote MuSCs activation and differentiation upon exposure to HDACi

The pan-HDACi Givinostat (Giv) is the first "epigenetic" drug that has been used in a clinical trial with DMD boys (Bettica *et al*, 2016). Histological analysis of muscles from patients treated with Giv showed increased regeneration, with a concomitant decrease in fibrosis and fat infiltration, akin to the effects previously observed in pre-clinical studies with mdx mice (the mouse model of DMD) treated with pan-HDACi, such as Giv or Trichostatin A (TSA) (Minetti *et al*, 2006; Consalvi *et al*, 2013). In addition to the histological analysis, we also obtained access to representative fresh biopsies from 2 DMD patients, before and after Giv treatment, from which we isolated by FACS two populations of our main interest—human MuSCs (CD11bneg, CD31neg, CD45neg, CD56/NCAMpos) and a population mesenchymal cells enriched in presumptive human FAPs (CD11bneg, CD31neg, CD45neg, CD56/NCAMneg). Figure EV1A shows that patient-derived human MuSCs (hMuSCs) could form myotubes when cultured *in vitro*; likewise, the cell population enriched in human FAPs (ehFAPs) could differentiate into adipocytes *in vitro*, when cultured in adipogenic medium. The availability of these patient-derived cells provides an unprecedented opportunity to evaluate the effect of HDACi on MuSC-FAPs interactions *ex vivo* and *in vivo*. *Ex vivo* experiments were performed by transwell co-culture of hMuSCs and ehFAPs from patients before the beginning of the clinical trial. In both patients, co-culture with ehFAPs slightly decreased hMuSC ability to differentiate into multinucleated myotubes (Fig 1A and B). This is in contrast with the reported ability of FAPs isolated from 2-month-old mdx mice to promote differentiation of MuSCs from the same animal (Mozzetta *et al*, 2013). The discrepancy between these results is likely accounted for by differences of DMD progression between human patients and mouse models, with 8- to 11-year-old patients enrolled in the clinical trial being at more advanced stages of disease progression, as also shown by the more pronounced fibrosis observed in their muscles, as compared to 2-month-old mdx mice. Exposure of ehFAPs to Giv (ehFAPs Giv Vitro) prior to co-culture with hMuSCs could increase the formation of hMuSC-derived myotubes to an extent comparable to that observed in hMuSCs isolated from patients after 1 year of Giv treatment *in vivo* (hMuSCs Giv) (Fig 1A

Figure 1. HDACi restores DMD FAP ability to support to MuSC differentiation into multinucleated myotubes.

A Representative images showing the myogenic differentiation, as assessed by immunostaining for MyHC (green), of human MuSCs (hMuSCs) isolated from muscle biopsies of DMD patients, either before the beginning of the clinical trial (hMuSCs (−)) or after 1 year of treatment with Givinostat (hMuSCs Giv (−)). Cells were cultured alone or (only for hMuSCs (−)) in transwell co-culture with FAPs isolated from the same patients and exposed *in vitro* to Giv (+ehFAPs Giv Vitro) or control vehicle (+ehFAPs). The upper panels represent myogenic differentiation of DMD-1 patient; bottom panels represent myogenic differentiation of DMD-2 patient. Dose and timing of Giv treatment as described in Bettica *et al* (2016). Scale bar = 50 μm.

B Graph showing the differentiation index of hMuSCs described in (A). Two technical replicates are shown.

C Representative images showing the myogenic differentiation of MuSCs isolated from 1.5-month-old mdx mice, as assessed by immunostaining for MyHC (green). MuSCs were cultured alone (−) or in transwell co-culture with mdx FAPs, which were pre-treated with DMSO or GW4869 (GW 10 mM added to FAPs 30 min before starting the co-culture with MuSCs). Scale bar = 50 μm.

D Graph showing the fusion index of MuSCs in the conditions described in (C), (n = 5, biological replicates). Star (*) indicates statistical analysis by Tukey's test relative to MuSCs cultured alone (−), $^{**}P < 0.01$; hash (#) indicates statistical analysis by Tukey's test relative to MuSCs in co-cultured with FAPs not treated (DMSO), $^{\#}P < 0.05$; § represents statistical analysis by two-way ANOVA test; $^{§§§}P < 0.001$.

E Representative images of PKH-67 (green) and DAPI (blue) staining in a transwell co-culture between MuSCs and FAPs isolated from 1.5-month-old mdx mice. FAPs exposed to PKH-67 prior to the co-culture with MuSCs. Scale bar = 50 μm.

F Graph showing the percentage of PKH-67-positive MuSCs after the co-culture with FAPs, (n = 3, biological replicates). Star (*) indicates statistical analysis by t-test; $^{****}P < 0.0001$.

G Representative images of myogenic differentiation of mdx MuSCs, as assessed by immunostaining for MyHC (green). MuSCs were cultured either alone (−) or incubated with EVs isolated from 1.5-month-old mdx mice (EVs-FAPs) treated with vehicle (CTR) or exposed to TSA *in vivo* (TSA) or *in vitro* (TSA vitro). Scale bar = 50 μm.

H Graph showing the fusion index of MuSCs in the condition described in (G), (n = 3, biological replicates). Star (*) indicates statistical analysis by Tukey's test on the % of $n > 5$ (% of nuclei that were MyHC$^+$ inside myotubes containing more than 5 nuclei) relative to MuSCs cultured alone (−), $^{**}P < 0.01$, $^{****}P < 0.0001$; hash (#) indicates statistical analysis by Tukey's test relative to EVs-FAPs CTR, $^{\#\#}P < 0.01$, $^{\#\#\#}P < 0.001$; ns = not significant; § represents statistical analysis by two-way ANOVA test, $^{§§§§}P < 0.0001$.

Data information: Nuclei were counterstained with DAPI (blue). All data correspond to the average ± SEM.

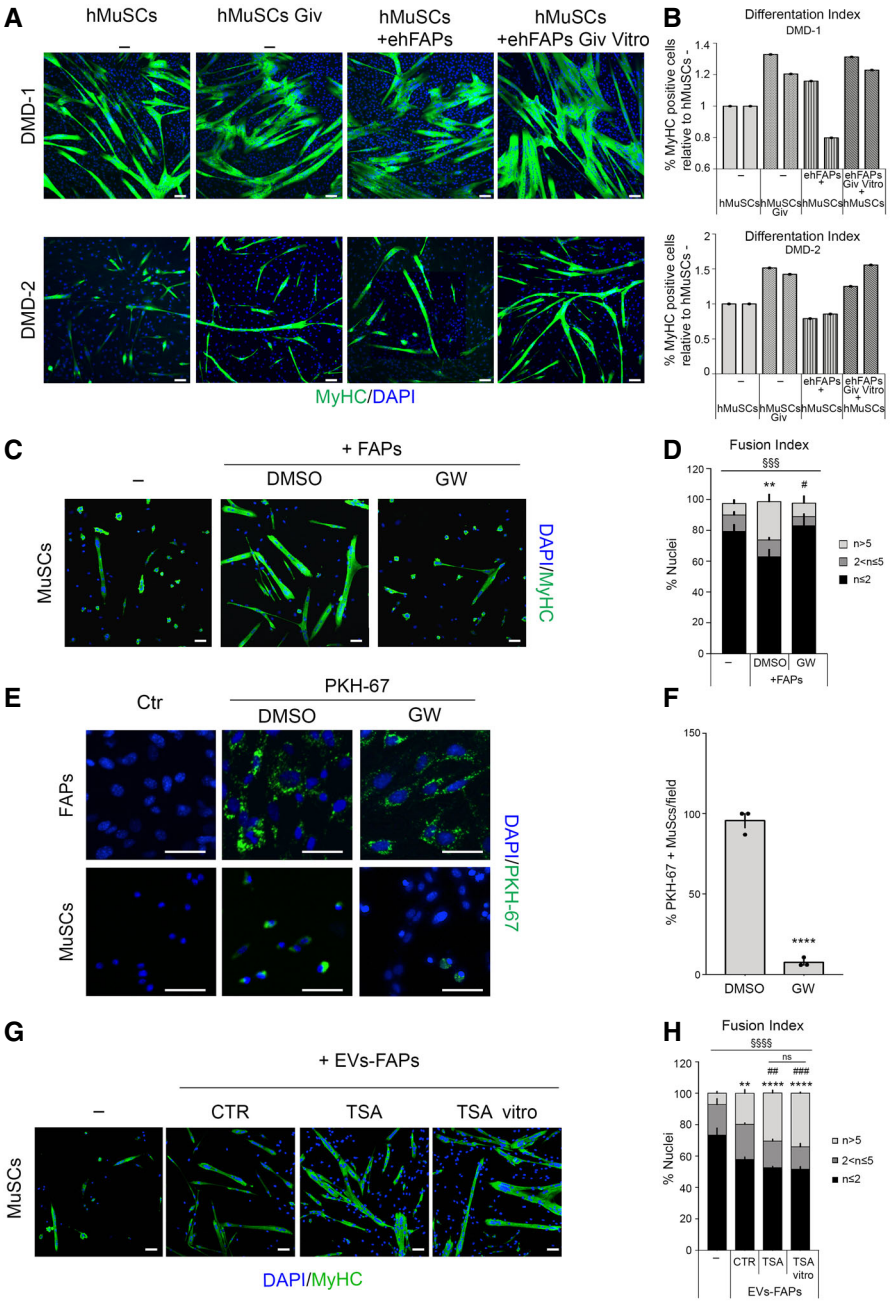

Figure 1.

and B). These data indicate that FAP's ability to support MuSC differentiation is compromised in muscles of DMD patients, but can be recovered upon treatment with HDACi.

To determine the identity of the extracellular mediators of the functional interactions between FAPs and MuSCs in DMD muscles, we performed transwell co-cultures of these cells isolated from the mouse model of Duchenne muscular dystrophy (DMD)—the mdx mice. FAPs were isolated from 1.5-month-old mdx mice and were co-cultured with MuSCs isolated from age-matched mdx mice. In transwell cultures, cells are separated by a membrane of 1 μm pore size that prevents direct cell contact, yet allows reciprocal transfer of soluble mediators—e.g., growth factors and cytokines, as well as extracellular vesicles (EVs), such as exosomes—that are exchanged between co-cultured cells. FAPs enhanced the ability of co-cultured MuSCs to differentiate into multinucleated myotubes, as compared to MuSCs cultured alone (Fig 1C and D), as previously reported (Mozzetta *et al*, 2013); however, exposure of FAPs to the neutral sphingomyelinase inhibitor GW4869, which selectively blocks exosome biogenesis (Trajkovic *et al*, 2008), prior to co-culture with MuSCs, abrogated FAP's ability to enhance MuSC differentiation into multinucleated myotubes (Fig 1C and D). This evidence indicates that EVs are essential contributors of FAP-mediated support to MuSC activity and implies that FAP-delivered EV/exosomes are transferred to MuSCs, whereby they influence MuSC biological properties.

We next isolated EVs from FAP's supernatant and analyzed their size distribution by dynamic light scattering (DLS) experiments. To this purpose, we have compared two purification procedures: (i) a commercially available Total Exosome Isolation™ precipitation Reagent (TEIR) and (ii) the current gold standard isolation method, which is based on differential ultracentrifugations (UC) (Théry *et al*, 2006; Van Deun *et al*, 2014). DLS analyses showed for both FAP-derived vesicle preparations an average hydrodynamic diameter of about 150 nm that is consistent with the standard size of exosomes (Fig EV1B) (Raposo & Stoorvogel, 2013). DLS analysis was also complemented with scanning electron microscopy (SEM) analyses of fixed TEIR-isolated EVs that showed round-shaped FAP-derived EVs ranging from 100 to 150 nm in size (Fig EV1C). The slight difference in size between SEM and DLS analyses can be explained by the fact that DLS measures the hydrodynamic diameter of native particles in dispersion and is inherently biased toward larger particles (Sokolova *et al*, 2011). Moreover, a Western blot analysis of the protein content showed that presumptive exosome markers were abundantly expressed in EVs TEIR isolated from FAP's supernatant, including Alix, Hsp70, and to a less extent Flotillin-1 and CD63 (Fig EV1D). EV preparation was cleared from contaminating cell organelles, as indicated by the absence of Calnexin, an ubiquitously expressed ER protein that was exclusively found in FAP's whole-cell fractions (WCL) (Fig EV1D). While these data demonstrate that FAP-derived EVs display typical features of mammalian exosomes (EV-TRACK Consortium *et al*, 2017), in this manuscript we will continue to refer to these nanoparticles as EVs.

To analyze the capacity of MuSCs to uptake FAP-derived EVs, we performed a transwell co-culture in which the potential cellular "source" of EVs—the FAPs—was transfected with the exosomal marker CD63 fused to GFP prior to transwell co-culture with the "acceptor" cells—the MuSCs. In this system, detection of GFP into MuSCs reveals the transfer of CD63-labeled EVs from FAPs to MuSCs. Figure EV1E shows that GFP signal was detected in FAPs after transfection with GFP-CD63, as well as in MuSCs co-cultured with FAPs previously transfected with GFP-CD63. By contrast, no GFP signal was detected in MuSCs co-cultured with FAPs previously transfected with a control plasmid (mock) (Fig EV1E). To further demonstrate the transfer of EVs from FAPs to MuSCs, we incubated FAPs with the lipidic dye (PKH-67) prior to transwell co-culture with MuSCs. PKH-67 is incorporated into newly generated EVs; hence, it can be used to trace EV passage from FAPs to acceptor cells. Indeed, PKH-67 staining was invariably detected in FAPs exposed to the dye as well as in recipient co-cultured MuSCs. On the other hand, prior exposure of FAPs to GW4869 almost completely prevented the detection of the signal in MuSCs (Fig 1E and F), demonstrating that FAP-derived EVs are uptaken by MuSCs.

To evaluate whether FAP-derived EVs could deliver regulatory signals to MuSCs, we incubated MuSCs with EVs isolated from the supernatant of FAPs from 1.5-month-old mdx mice (CTR). FAP-derived EVs increased the ability of MuSCs to form multinucleated myotubes (Fig 1G and H—compare CTR to untreated -MuSCs (−)). To determine whether EVs mediate the ability of HDACi to enhance FAP's support to MuSC differentiation, we incubated MuSCs with EVs that were purified from FAPs of mdx mice exposed for 15 days to TSA. These EVs further increase the formation of multinucleated myotubes from MuSCs, as compared to EVs from FAPs of CTR vehicle-treated mdx (Fig 1G and H—compare TSA to CTR). We next sought to evaluate whether HDACi could directly promote release of pro-myogenic EVs, by exposing cultures of FAPs isolated from vehicle-treated mdx mice to TSA (TSA vitro). Exposure of FAPs to TSA *ex vivo* led to the release of EVs that promoted MuSC-mediated formation of multinucleated myotubes to an extent comparable to that observed with EVs from FAPs isolated from mdx mice treated *in vivo* with TSA (Fig 1G and H—compare TSA vitro to untreated). These results are consistent with data from human DMD patients shown in Fig 1A and B.

We also evaluated whether HDACi could increase the abundance of FAP-derived EVs. To this purpose, we exposed the same number of FAPs isolated from vehicle-treated mice to TSA *ex vivo* and quantified the number of EVs released in the supernatant. Figure EV1F and G shows that TSA increased the abundance of EVs in the supernatant of FAP cultures, as compared to CTR-treated FAPs. As the supernatant was collected from the same number of cells in each condition, the increased amounts of EVs did not depend on the effect of TSA on cell proliferation, but likely reflected an increased cellular output of EVs.

Enrichment of miR-206 in interstitial EVs correlates with compensatory regeneration of DMD muscles and treatment with HDACi

We next investigated whether FAP-derived EVs could be detected in regenerating muscles, in physiological (acute injury) or pathological (DMD) conditions. To this purpose, we performed *in situ* immunofluorescence for CD63, an integral membrane protein enriched in EVs, on muscle sections from young wild-type (WT) unperturbed (CTR) or regenerating muscles (4-day post-injury cardiotoxin (CTX) injection) and from mdx mice at different stages of disease progression (i.e., 1.5-month-old or 12-month-old mice). We also included sections of muscles from mdx mice that were exposed or not to the TSA, which reportedly promotes regeneration in young, but not old, mdx mice (Mozzetta *et al*, 2013; Saccone *et al*, 2014). This analysis revealed sporadic CD63 signal in WT unperturbed and old mdx muscles, while a dramatic increase in CD63 signal was observed in regenerating WT and mdx young muscles (Fig EV2A and B). Interestingly, in all experimental conditions the vast majority of CD63 signal was invariably detected in the interstitium between regenerating, embryonal eMyHC-positive fibers, and largely overlapped with interstitial Sca1 signal, which identifies putative FAP cells. Notably, muscles of mdx young mice exposed to TSA showed a significant increase in CD63-positive interstitial signal, as compared to young mdx CTR muscles, with levels comparable to those observed in regenerating WT muscles (Fig EV2A and B). By contrast, TSA treatment could not increase the CD63 signal in the interstitium of muscles from 1-year-old mdx mice, which have been previously shown to be resistant to the beneficial effects of HDACi (Mozzetta *et al*, 2013; Saccone *et al*, 2014). The overlap between interstitial CD63 and Sca1 signals, and the close proximity to eMyHC-positive regenerating myofibers, together with the differential response of young versus old mdx muscles to HDACi, suggest that FAP-derived EVs could be implicated in HDACi-mediated activation of MuSCs to regenerate dystrophic muscles, as previously indicated by transwell co-culture experiments (Mozzetta *et al*, 2013).

Previous works have implicated microRNA (miRs), as mediators of exosome-regulated biological processes (Valadi *et al*, 2007; Collino

et al, 2010; Montecalvo *et al*, 2012; Vlassov *et al*, 2012; Nakamura *et al*, 2015; Fry *et al*, 2017). To investigate miR contribution to the ability of FAP-derived EVs to regulate MuSC activity, we first determined whether FAP-derived EVs could transfer RNA to MuSCs, by using fluorescent acridine orange (AO)—a specific nucleic acid staining. AO-labeled FAP-derived EVs were incubated with freshly isolated MuSCs. Confocal microscopy analysis revealed the presence of AO-labeled intracellular RNA dots inside recipient MuSCs, both within and outside the nuclear membrane (Fig EV3A). We have previously shown that HDACi extensively changes the miR expression pattern in FAPs from mdx muscles (Saccone *et al*, 2014). Therefore, we sought to further investigate the functional impact of siRNA-mediated blockade of miR biogenesis on muscle regeneration. We evaluated the effect of siRNA-mediated knockdown of Drosha, the RNA-specific endoribonuclease required for microRNA biogenesis, on functional interactions between FAPs isolated from HDACi-treated young mdx mice and MuSCs isolated from control-treated young mdx mice. siRNA efficiently down-regulated (by about 60%) Drosha expression in FAPs (Fig 2A) and drastically reduced the ability of TSA-treated FAPs to enhance MuSC-mediated formation of multinucleated myotubes in transwell co-culture (Fig 2B and C). We then determined the identity of the miRs within FAP-derived EVs, by performing a TaqMan-based miR expression microarray using EVs purified from the supernatant of FAPs isolated from mdx mice treated for 15 days with TSA or control vehicle (CTR). This analysis identified several miRs up-regulated in EVs from TSA-treated mdx mice. We annotated the top 14 miRs significantly up-regulated in FAPs from TSA-treated mdx mice (Figs 2D and EV3B), including miRs that have been previously implicated in the regulation of skeletal myogenesis (Greco *et al*, 2009; Liu *et al*, 2012; Wang *et al*, 2012; Yamamoto *et al*, 2012; Wang, 2013; Guess *et al*, 2015; Nakamura *et al*, 2015; Zhao *et al*, 2016). Ingenuity pathway analysis (IPA) revealed a number of regulatory pathways potentially affected by these miRs and implicated in the control of MuSCs (Fig EV3C). Interestingly, RNA-seq data generated from MuSCs isolated from mdx mice treated with TSA versus control vehicle revealed the activation of top pathways (e.g., *Notch*, *JAK-STAT*) that were also predicted by IPA of the up-regulated miR in EVs from FAPs of TSA-treated mdx mice (Fig EV3D). Among the TSA-induced EV-miRs, the most up-regulated (17.06-fold) was the muscle-specific (myomiR) miR-206-3p (herein indicated as miR-206)—a central component of skeletal muscle regeneration (Liu *et al*, 2012; Ma *et al*, 2015), and HDACi-activated network in dystrophic muscles (Cacchiarelli *et al*, 2010; Saccone *et al*, 2014). Of note, transgenic overexpression of miR-206 has been successfully exploited as tool for the treatment of DMD and other muscular disorders (Williams *et al*, 2009; Liu *et al*, 2012; Fry *et al*, 2017). Interestingly, *in situ* hybridization analysis of muscle biopsies from DMD patients at various ages revealed increased levels of interstitial miR-206, as compared to control biopsies (from non-DMD boys) (Fig 2E and F). This analysis also showed a progressive reduction in interstitial miR-206 along with the disease progression in coincidence with the exhaustion of the regenerative activity and the increased severity of fibrosis (Fig 2G–J). The same pattern could also be observed in mdx mice, in which an abundant miR-206 signal was detected in the interstitium of tibialis anterior muscles, overlapping with the immunofluorescence staining of the FAP's marker Sca-1 (Fig 3A and B).

We next investigated whether exposure to HDACi could increase the interstitial amount of intravesicular miR-206 to the levels observed at earlier stages of disease progression. Treatment of young mdx mice (1.5 months of age) with TSA, which promotes regeneration and inhibits fibrosis (Mozzetta *et al*, 2013; Saccone *et al*, 2014), could increase the amount of interstitial miR-206 signal associated with Sca-1 staining, which was used to identify putative FAPs (Fig 3A and B). We performed a quantitative assessment (by qPCR) of EV-miR-206, upon isolation of whole tibialis anterior (TA) muscles from TSA-treated mdx muscle or control vehicle-treated mdx mice, followed by mechanic dissociation and EV purification (Aswad *et al*, 2014). This procedure enriches for interstitial material, as it minimizes EV content in myofibers, and showed a ~5-fold increase in miR-206 in TSA-treated mdx muscle as compared to control-treated (Fig 3C).

We then performed *in situ* hybridization analysis of miR-206 expression and localization in muscle biopsies from DMD patients, before or after the treatment with Giv. We used muscle sections available from 18 patients, among the 19 DMD boys enrolled in this clinical trial, as one dropped off from the trial. In these patients, we found an increased abundance of miR-206 after Giv treatment (Fig 3D and E). Of note, the miR-206 signal was detected in the interstitial space and was almost invariably juxtaposed to CD90 signal, which identifies human FAPs (see merge picture, in which the IF and hybridization signals are merged, the CD90 signal turns purple, and the miR-206 signal remains violet). This suggests that FAPs are the main source of the interstitial miR-206 in DMD muscles. Consistently, we detected 12- to 16-fold increase in miR-206 in the EVs from ehFAPs of the biopsies available from our two DMD patients (Fig 3F).

Interestingly, the miR-206 signal was also detected in myofibers of regenerating fibers of DMD patients (Fig 2E) and mdx mice (Fig 3A), but was much attenuated in fibers of DMD patients at late stage of disease or in control human muscle sections (Figs 2E–G and 3D). The overall pattern of miR-206 staining inside myofibers and within the interstitial spaces of regenerating areas of DMD muscles is consistent with the established role of miR-206 in developmental and post-natal myogenesis (Yuasa *et al*, 2008; Cacchiarelli *et al*, 2010; Koutsoulidou *et al*, 2011). Accordingly, increased levels of miR-206 could be detected in the fibers of mdx mice as well as DMD patients treated with HDACi (see Fig 3D–F). This is consistent with the general trend of increased muscle regeneration observed in DMD patients after 1 year of treatment with Giv (Bettica *et al*, 2016) and in mdx mice treated with Giv (Consalvi *et al*, 2013) or other HDACi (Minetti *et al*, 2006; Colussi *et al*, 2008).

EV-miRs cooperatively promote compensatory regeneration while reducing fibrosis and inflammation in dystrophic muscles

The enrichment of interstitial EVs with increased amounts of miR-206 in regenerating DMD muscles suggests that FAP-derived EVs could transfer miR-206 to MuSC to promote compensatory regeneration. While miR-206 transfer by exosomes from MuSCs to interstitial fibroblasts has been recently described as a mechanism to hamper the formation of fibrotic scars during skeletal muscle hypertrophy (Fry *et al*, 2017), the reciprocal process—that is, transfer of miR-206 from FAPs to MuSCs—has not been described so far. We therefore explored the potential transfer of miR-206 from FAPs to MuSCs,

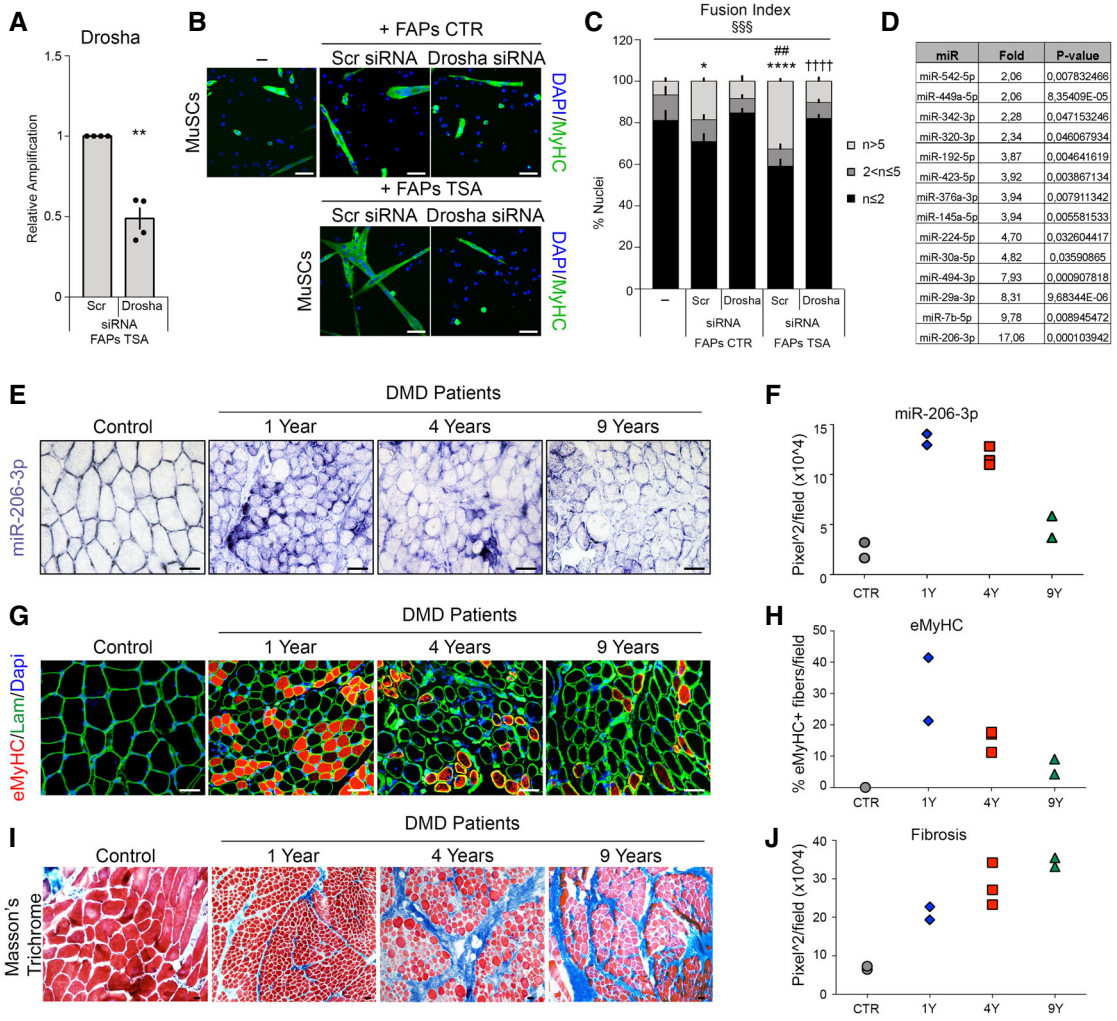

miR	Fold	P-value
miR-542-5p	2,06	0,007832466
miR-449a-5p	2,06	8,35409E-05
miR-342-3p	2,28	0,047153246
miR-320-3p	2,34	0,046067934
miR-192-5p	3,87	0,004641619
miR-423-5p	3,92	0,003867134
miR-376a-3p	3,94	0,007911342
miR-145a-5p	3,94	0,005581533
miR-224-5p	4,70	0,032604417
miR-30a-5p	4,82	0,03590865
miR-494-3p	7,93	0,000907818
miR-29a-3p	8,31	9,68344E-06
miR-7b-5p	9,78	0,008945472
miR-206-3p	17,06	0,000103942

Figure 2. Increased amounts of miR-206-3p in DMD muscles associate with muscle regeneration and inversely correlate with disease progression.

A Graph showing the relative expression of Drosha in FAPs after Drosha down-regulation by siRNA (n = 4, biological replicates). Values correspond to the average ± SEM. Star (*) indicates statistical analysis by t-test relative to FAPs TSA treated and transfected with scramble (Scr); $^{**}P < 0.01$.

B Representative images of myogenic differentiation of MuSCs assessed by immunostaining for MyHC (green). MuSCs were cultured alone (–) or in transwell co-culture with FAPs isolated from mdx mice treated either with vehicle (+FAPs CTR) or TSA (0.6 mg/kg/day for 15 days by i.p.) (+FAPs TSA), and transfected with scramble (Scr siRNA) or Drosha siRNA (Drosha siRNA) prior to co-culture with MuSCs. Scale bar = 50 μm.

C Graph showing the fusion index of MuSCs in the conditions described in (B) (n = 4, biological replicates). Values correspond to the average ± SEM. Star (*) indicates statistical analysis by Tukey's test relative to MuSCs alone (–); $^{*}P < 0.05$, $^{****}P < 0.0001$. Hash (#) indicates statistical analysis by Tukey's test relative to MuSCs in co-culture with FAPs CTR transfected with scramble (Scr); $^{\#\#}P < 0.01$. Cross (†) means Tukey's analysis compared to MuSCs in co-culture with FAPs TSA transfected with scramble (Scr): $^{\dagger\dagger\dagger\dagger}P < 0.0001$. § represents statistical analysis by two-way ANOVA test. $^{\S\S\S}P < 0.001$.

D Table representing a manually assembled list of microRNAs revealed by microarray analysis and statistically induced by TSA in FAP-derived EVs.

E Representative images of miR-206-3p (violet) immunohistochemistry in vastus medialis bioptic samples of control and DMD patients at different ages: 1 year (n = 2), 4 years (n = 3), and 9 years old (n = 2).

F Graph representing miR-206-3p violet area quantification relative to (E).

G Representative images of immunofluorescence for eMyHC (red) and laminin (green) in conditions described in (E).

H Graph showing the percentage of eMyHC-positive fibers of condition described in (G).

I Representative images of Masson's trichrome staining in conditions described in (E).

J Graph showing the fibrotic area quantification of conditions described in (I).

Data information: For (E, G, I) Scale bar = 50 μm.

through EVs, within the context of the mdx muscles. To this purpose, we quantified MuSC's uptake of FAP-derived EVs *in vivo*, by tracing EVs with PKH-67 labeling. EVs were first purified from FAPs isolated from mdx mice previously treated with TSA (EVs-FAPs TSA) and then exposed to PKH-67, prior to their transplantation into tibialis anterior (TA) muscles. FACS analysis showed that 17.2% of the whole population of cells isolated from transplanted TA muscle incorporated PKH-67-labeled EVs (Fig 4A, left panel). Among them, we found that about 2% of FACS-isolated MuSCs were detected positive for PKH-67 signal (Fig 4A, right

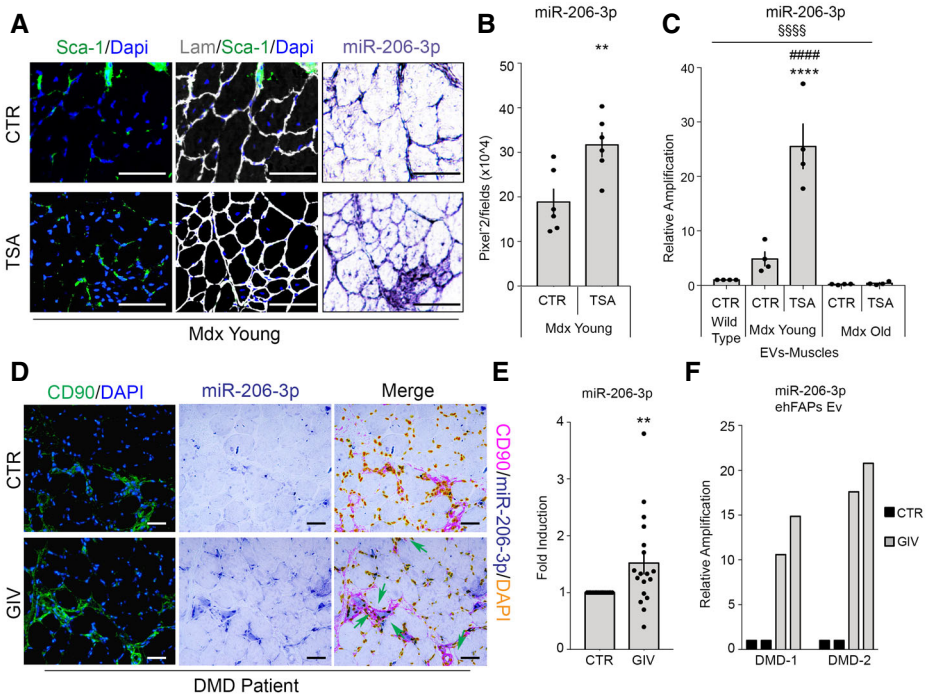

Figure 3. HDACi increases miR-206-3p amounts in EVs from DMD FAPs.

A Representative images of Sca-1 (green), laminin (white), DAPI (blue) immunofluorescence, and miR-206-3p (violet) immunohistochemistry on 10 μM sequential cryo-sections of tibialis anterior (TA) of young mdx mice (CTR) and after TSA treatment (TSA) (0.6 mg/kg/day for 15 days by i.p.) (n = 6). Scale bar = 25 μm.

B Graph showing the quantifications of miR-206-3p violet area relative to conditions indicated in (A). Star (*) indicates t-test analysis $^{**}P < 0.01$.

C Graph representing the miR-206-3p relative expression in EVs isolated from muscle interstitium of tibialis anterior from wild-type (CTR), mdx young, and old mice (control (CTR) and TSA treated) (n = 4). Star (*) indicates Tukey's analysis compared to wild-type mice (CTR), $^{****}P < 0.0001$; hash (#) indicates Tukey's analysis compared to mdx young CTR, $^{\#\#\#\#}P < 0.0001$. § represents statistical analysis by ANOVA test. $^{§§§§}P < 0.0001$.

D Representative images of CD90 (green), DAPI (blue), and miR-206-3p (violet) immunohistochemistry in brachial biceps bioptic samples of DMD patient before (CTR) and after Givinostat treatment (GIV). Scale bar = 50 μm.

E Graph showing the quantifications of miR-206-3p violet area measured as pixel^2/field relative to the experimental points indicated in (D) (n = 18, biological replicates). Star (*) indicates t-test analysis. $^{**}P < 0.01$.

F Graph showing the relative expression of miR-206-3p in EVs isolated from a human population of muscle-resident cells enriched in FAPs (ehFAPs) isolated from biopsies of two DMD patients (DMD-1 and DMD-2) before (CTR) and after (GIV) Givinostat treatment. Two technical replicates are shown.

Data information: Nuclei were counterstained with DAPI (blue). All data for (B, C, and E) correspond to the average ± SEM, while the data for (F) correspond to the average ± SD.

panel, and Fig 4B). We argue that such a low percentage of PKH-67-positive MuSCs detected underestimates the actual rate of MuSC incorporation of FAP-derived EVs, as it is intrinsically biased by the loss of PKH-67-positive MuSCs, due to the dye dilution once they proliferate and/or differentiate into large multinucleated myofibers. Consistent with EV-mediated transfer of miR-206 from FAPs to MuSCs in DMD muscles exposed to HDACi, MuSCs that incorporated PKH-67-labeled EVs exhibited a fivefold increase in miR-206 (Fig 4C), further indicating that FAP-derived EVs significantly increase the intracellular amount of miR-206 in MuSCs. Furthermore, global inhibition of miR biogenesis in FAPs, by Drosha knockdown via RNA interference (siRNA) prior to EV isolation and injection, was sufficient to prevent the increase in miR-206 in PKH-67-positive MuSCs isolated from transplanted muscles (Fig 4C). Likewise, in a parallel experiment, inhibition of EV biogenesis by exposure to GW4869 abrogated miR-206 transfer from TSA-treated mdx FAPs to co-cultured MuSC transwell plates (Fig EV4A). When considered with the previous report from Fry *et al* (2017), this finding is consistent with a model of reciprocal exchange of miRs between FAPs and MuSCs.

We next monitored the effect of EVs-FAP TSA on parameters of disease progression in mdx mice upon EV transplantation. Since HDACi exert beneficial effects in mdx mice, by promoting compensatory regeneration and by reducing fibrosis and inflammation (Minetti *et al*, 2006), we sought to evaluate to what extent these effects are accounted for by FAP-derived EVs. To this purpose, we compared the ability of intramuscular (i.m.) injection of EVs purified from FAPs isolated from mdx mice that were previously treated with TSA (EVs-FAPs TSA) or vehicle (EVs-FAPs CTR) to stimulate regeneration, and reduce fibrosis and inflammation. The effect was compared to systemic exposure to TSA (or vehicle control), which was administered via daily intraperitoneal injection for 21 days. Intramuscular injection of EVs was repeated every 7 days for 21 days, in order to allow a direct comparison with the systemic exposure to TSA. Within this context, we evaluated the specific contribution of miR-206 to the effects of FAP-derived EVs on mdx mice, by transfecting with antagomiR-206 FAPs isolated from TSA-

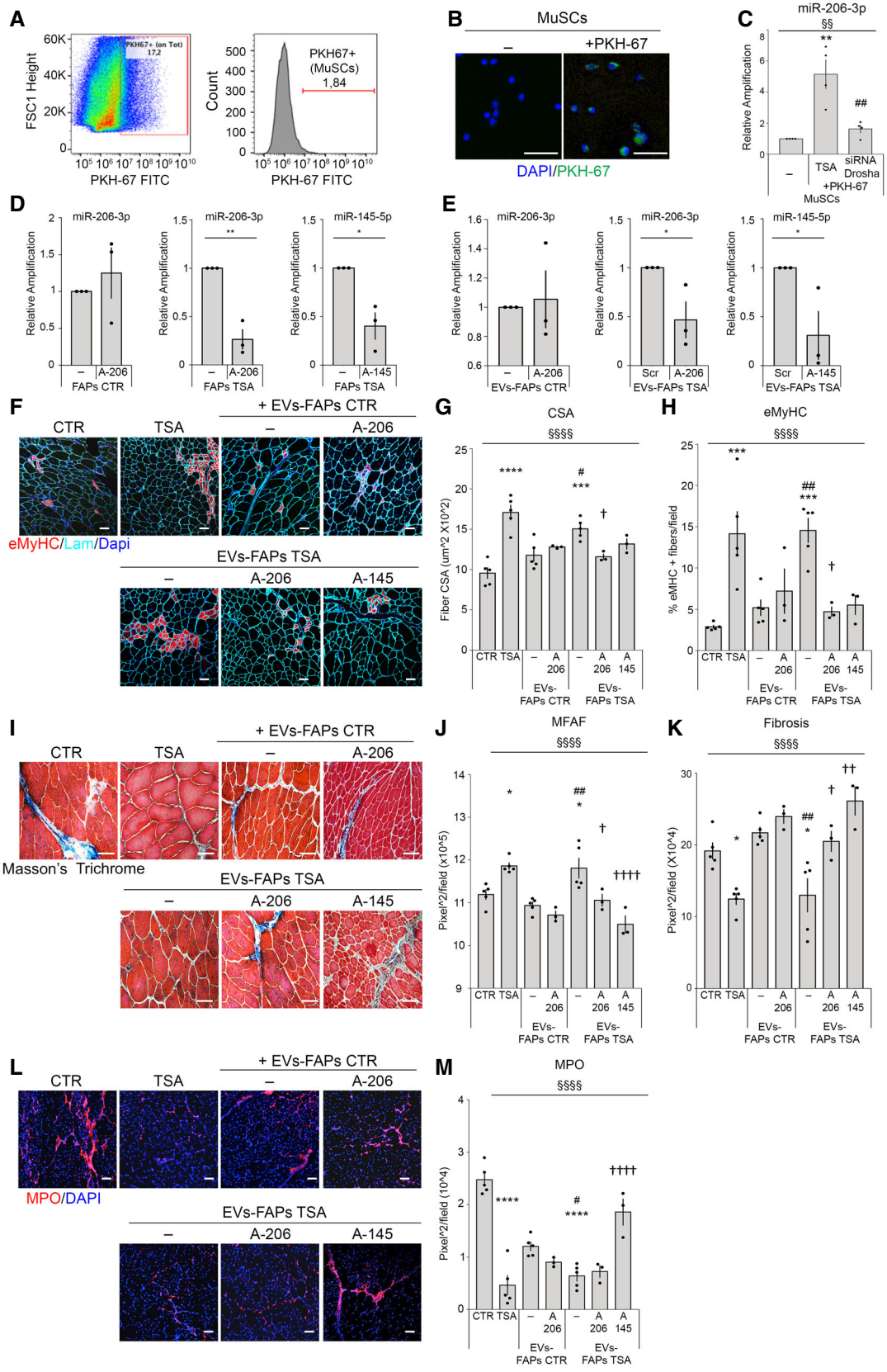

Figure 4.

Figure 4. FAP-derived EVs promote regeneration and inhibit fibrosis and inflammation in dystrophic muscles of mdx mice.

A Flow cytometric analysis of mdx muscles injected with PKH67-labeled EVs isolated from FAPs of 1.5-month-old mdx mice exposed to TSA. The left panel shows the percentage of PKH-67-positive cells in whole muscle. The right panel shows the percentage of the PKH-67-positive MuSCs.

B Representative images of PKH-67 (green) and DAPI (blue) staining in MuSCs freshly isolated from muscles previously injected with PKH67-labeled EVs. Scale bar = 25 μm.

C Graph showing the relative expression of miR-206-3p in MuSCs isolated as described in (A, B) and in MuSCs from muscles injected with PKH67-labeled EVs isolated from FAPs of 1.5-month-old mdx mice exposed to TSA, and then transfected or not with Drosha siRNA (siRNA Drosha) (n = 4). Star (*) means significance relative to MuSCs that not uptake PKH67-labeled EVs, $^{**}P < 0.01$. Hash (#) means significance compared to MuSCs that uptake EVs-FAPs TSA, $^{\#\#}P < 0.01$. § indicates ANOVA, $^{\S\S}P < 0.01$.

D Graph showing the expression levels of miR-206-3p and miR-145-5p in FAPs treated or not with TSA after antagomiR treatment (n = 3, biological replicates). Star (*) indicates statistical analysis by t-test relative to FAPs (–); $^{*}P < 0.05$, $^{**}P < 0.01$.

E Graph showing the expression levels of miR-206-3p and miR-145-5p in FAP-derived EVs treated or not with TSA after antagomiR treatment (n = 3, biological replicates). Star (*) indicates statistical analysis by t-test relative to FAPs (–); $^{*}P < 0.05$.

F–M Stainings and relative measurements on tibialis anterior muscle transversal sections of 1.5-month-old mdx mice treated daily for 21 days with intraperitoneal injection of vehicle (CTR) or TSA, or once a week with intramuscular injections (tibialis anterior) of EVs derived from FAPs (EVs-FAPs) exposed or not to TSA *in vivo* (EVs-FAPs CTR (–), EVs-FAPs TSA (–)) EVs derived from FAP control transfected with the antagomiR-206 (EVs-FAPs CTR A-206) and of EVs-FAPs TSA transfected with antagomiR-206 and antagomiR-145 (EVs-FAPs TSA A-206, EVs-FAPs TSA A-145). EVs were injected every 7 days and sacrificed after 21 days of treatment (n = 5 for CTR, TSA EVs-FAPs CTR, and EVs-FAPs TSA, while for antagomiRs, n = 3, biological replicates). (F) Representative images of immunofluorescence for embryonic myosin heavy chain (eMyHC—red) and laminin (Lam—cyan) stainings. Scale bar = 50 μm. (G) Graph showing the quantification of cross-sectional area (CSA). (H) Graph showing the quantification of muscle regeneration (eMyHC). (I) Representative images of Masson's trichrome staining. Scale bar = 50 μm. (J) Graph showing the quantifications of muscle fiber area fraction (MFAF). (K) Graph showing the quantifications of fibrotic area. (L) Representative images of myeloperoxidase staining (MPO—red). Scale bar = 50 μm. (M) Graph showing the quantifications of inflammation (MPO).

Data information: Nuclei were counterstained with DAPI (blue). Statistical analysis by ANOVA and Tukey's test. All data correspond to the average ± SEM. In (A-H), star (*) means significance compared to CTR, $^{*}P < 0.05$, $^{**}P < 0.01$; $^{***}P < 0.001$; $^{***}P < 0.0001$, while hash (#) means significance compared to EVs-FAPs CTR (–), $^{\#}P < 0.05$, $^{\#\#}P < 0.01$, and (†) means significance to EVs-FAPs TSA (–), $^{\dagger}P < 0.05$, $^{\dagger\dagger}P < 0.01$, $^{\dagger\dagger\dagger\dagger}P < 0.0001$. § indicates significance by ANOVA test; $^{\S\S\S}P < 0.001$; $^{\S\S\S\S}P < 0.0001$.

treated mice (EVs-FAPs A-206) prior to EV isolation and injection into tibialis anterior of mdx mice. As an internal control, we sought to transfect FAPs with antagomiRs against another HDACi-induced miR in FAP-derived EVs that has a spectrum of targets non-overlapping with miR-206. To this purpose, we used antagomiRs against miR-145 (A-145), which displayed a fourfold up-regulation in EVs derived from FAPs of HDACi-treated mdx mice (Fig 2D) and targets key mediators of inflammation, such as IL1, IL6, and TGFbeta signaling (Tahamtan *et al*, 2018). Transfection of A-206 or A-145 in FAPs specifically reduced the expression levels of miR-206 or miR-145, respectively, in FAPs (Fig 4D) as well as in FAP-derived EVs (Fig 4E). This effect was observed only after miR induction upon FAP exposure to TSA, but not in untreated FAPs, consistent with the almost undetectable levels of these miRs in FAPs under basal conditions.

Mdx muscles injected with EVs-FAP TSA showed an increase in embryonic-MyHC-positive myofibers (eMyHC) and cross-sectional area (CSA), comparable to the increase observed in the muscles of mdx mice following systemic exposure to TSA (Fig 4F–H). Likewise, EVs-FAPs TSA i.m. injection and systemic delivery of TSA showed a comparable ability to increase muscle fiber area fraction (MFAF) and reduce fibrosis (Figs 4I–K and EV4B and C), as well as inflammation, as determined by reduction of myeloperoxidase (MPO)-positive areas, in mdx muscles (Fig 4L and M). EVs-FAPs TSA A-206 showed a reduced ability to stimulate muscle regeneration (Fig 4F–H) and inhibit fibrosis (Fig 4I–K), but maintained their anti-inflammatory effects, indicating a selective contribution of miR-206 in promoting regeneration and reducing fibrosis. By contrast, the anti-inflammatory effects were lost in EVs-FAPs TSA A-145 (Fig 4L and M). Notably, EVs-FAPs TSA A-145 also showed reduced pro-myogenic (Fig 4F–H) and anti-fibrotic effects (Fig 4I–K), as compared to control EVs-FAPs TSA. It is likely that loss of pro-myogenic and anti-fibrotic activities in EVs-FAPs TSA A-145 is secondary to the loss of the anti-inflammatory effect, as inflammation typically inhibits myogenic regeneration and promotes fibrosis. Overall, these data show that the therapeutic effect exerted by EVs from HDACi-treated FAPs in mdx mice results from the combinatorial, and often redundant, activities of multiple intra-EV miRs up-regulated by HDACi.

We also investigated whether the HDACi-mediated up-regulation of miRs in FAP-derived EVs is direct and cell-specific. We found that direct exposure of FAPs to TSA *ex vivo* induced an up-regulation of the same miRs detected by microarray from EVs isolated from the supernatant of FAPs derived by TSA-treated mdx mice *in vivo* (see Fig 2D), with a comparable magnitude (Fig EV4D). Moreover, *ex vivo* exposure to TSA was used to determine whether HDACi-induced up-regulation of miR-206 in EVs could be observed also in muscle-derived cell types that typically express miR-206—i.e., MuSCs and myotubes. Figure EV4E–H shows that upon *ex vivo* exposure to TSA, only FAP-derived EVs exhibited up-regulation of miR-206, although TSA could increase the transcription of miR-206 in both MuSCs and myotubes. These data indicate that transcriptional up-regulation of miRs by HDACi is not sufficient to increase their levels in EVs and points to the importance of cell type-specific post-transcriptional regulation of miR incorporation into EVs.

EVs isolated from FAPs of HDACi-treated dystrophic muscles are required to promote MuSCs activation and amplification

To gain mechanistic insights into the pro-myogenic activity of EVs derived from FAPs of HDACi-treated mdx mice, we searched for putative target genes of miR-206 that matched with down-regulated genes in our RNA-seq datasets obtained from MuSCs of TSA-treated mdx mice. A downstream analysis was carried out only for miR-206 targets that have been already annotated or predicted with high confidence. Ingenuity pathway analysis (IPA) revealed a potential effect of miR-206 on various signaling pathways involved in muscle development and disease, including *Utrophin* (UTRN), *Pax7*, and *Notch3* (Rosenberg *et al*, 2006; Chen *et al*, 2010; Gagan *et al*, 2012; Amirouche *et al*, 2014) (Fig EV5A). We decided to focus on miR-206 regulation of *Notch3*, as negative regulator of MuSC differentiation,

because previous work demonstrated that miR-206 down-regulation of *Notch3* promotes MuSC differentiation (Gagan *et al*, 2012). We therefore purified EVs from FAPs isolated from TSA- or control (vehicle)-treated 1.5-month-old mdx mice for 21 days and evaluated their effect on MuSC ability to form myotubes, while monitoring the expression levels of *Notch3* and *Notch1*. EVs from FAPs of TSA-treated mdx mice increased MuSC ability to form multinucleated myotubes, and this effect was abrogated by antagomiR-mediated depletion of miR-206 in FAP-derived EVs (Fig 5A and B). In keeping with the opposite roles of Notch members in MuSC activation (Kitamoto & Hanaoka, 2010), we reasoned that selective down-regulation of *Notch3* in MuSCs upon incorporation of FAP-derived EVs could promote MuSC activation and self-renewal. Indeed, while *Notch3* and *Notch1* transcripts were both reduced in MuSCs isolated from mdx mice treated with TSA, we observed a selective down-regulation of *Notch3* transcripts in MuSCs isolated from control-treated mice and cultured with EVs derived from FAPs of TSA-treated mdx mice (Fig 5C and D).

We next evaluated the effect of EVs derived from FAPs of HDACi-treated or control-treated mdx mice on MuSCs within single fibers isolated from WT mice. Freshly isolated single muscle fibers from tibialis anterior, extensor digitorum longus, gastrocnemius and soleus of C57BL/6J mice were incubated with FAP-derived EVs or whole conditioned media, and their effect on MuSCs was evaluated by monitoring the expression of Pax7, MyoD, and DNA synthesis (EdU incorporation). In this experimental setting, the uptake of FAP-derived EVs by MuSCs from single fibers was first confirmed by staining of lipidic dye PKH-67 used to label purified vesicles (Fig 5E). Figure 5F and G shows that the whole supernatant derived from FAPs of control-treated mdx mice increased the number of $Pax7^+/MyoD^+$ MuSCs that showed enhanced DNA synthesis (Edu^+) and could be therefore considered activated MuSCs (Zammit *et al*, 2004). Indeed, nearly 100% of the EdU^+ nuclei were also $Pax7^+/MyoD^+$. Moreover, the whole supernatant derived from FAPs of TSA-treated mdx mice could further augment this effect. While a drastic reduction in the number of quiescent ($Pax7^+$ $MyoD^-$) and differentiation-committed MuSCs ($Pax7^-$ $MyoD^+$) was observed upon incubation with the whole supernatant of FAPs isolated from control-treated mdx mice and pre-exposed to GW4869, the number of $Pax7^+/MyoD^+$ MuSCs with high DNA synthesis (Edu^+) was not altered in these conditions (Fig 5F and G). By contrast, GW4869 treatment of FAPs from TSA-treated mdx mice drastically reduced the ability of the whole supernatant to increase all MuSC populations as well as their proliferation (Fig 5F and G). These data indicate that the ability of FAPs from HDACi-treated mdx mice to promote expansion of MuSCs depends on EVs. Indeed, only EVs from FAPs of TSA-treated (but not from control-treated) mdx mice increased the number of $Pax7^+/MyoD^+$ MuSCs (Fig 5F and G). We then investigated the relative contribution of miR-206 in mediating the ability of EVs isolated from FAPs of TSA-treated mdx mice to support MuSC activation, expansion, and differentiation. AntagomiR-mediated depletion of miR-206 drastically reduced the ability of EVs isolated from FAPs of TSA-treated mice to support the expansion of $Pax7^+/MyoD^+$ as well as $Pax7^-/MyoD^+$ MuSCs (Fig 5F and G). This result demonstrates the essential function of miR-206 in mediating HDACi ability to promote functional interactions between dystrophic FAPs and MuSCs.

Discussion

Defining the identity of extracellular mediators that coordinate the activities of the cellular components of the MuSC niche is a major challenge in regenerative medicine, as it might inspire selective interventions toward promoting compensatory regeneration of diseased muscles, while eliminating the most unfavorable outcome of disease progression, such as maladaptive repair by deposition of

Figure 5. EVs from FAPs *in vivo* exposed to TSA promote MuSC differentiation, expansion, and asymmetric division.

A Representative images of myogenic differentiation of MuSCs assessed by immunostaining for MyHC (green). Nuclei were counterstained with DAPI (blue). MuSCs were cultured alone (–) or with EVs (EVs-FAPs) isolated from FAPs *in vivo* exposed or not to TSA (CTR and TSA) and transfected or not with antagomiR-206 ((–) and A-206). (n = 7 for all samples, but antagomiR's samples n = 3, biological replicates). Scale bar = 50 μm.

B Graph showing the fusion index of MuSCs in the condition described in (A). Star (*) indicates statistical analysis by Tukey's test relative to MuSCs cultured alone (–), $^*P < 0.05$, $^{****}P > 0.0001$; hash (#) means significance compared to EVs-FAPs CTR (–), $^{\#\#\#}P < 0.001$; and (†) means significance to EVs-FAPs TSA (–), $^{\dagger\dagger\dagger\dagger}P < 0.0001$. § indicates significance by ANOVA test; $^{\S\S\S\S}P > 0.0001$.

C Graph relative to Notch3 expression in MuSCs isolated from 1.5-month-old mdx mice treated with either vehicle (CTR) or TSA (TSA), and in EVs derived from FAPs (EVs-FAPs) isolated from 1.5-month-old mdx mice treated with either vehicle (CTR) or TSA (TSA) (n = 3). Star (*) indicates statistical analysis by Tukey's test relative to mdx vehicle-treated mdx mice (CTR); $^*P < 0.05$. Hash (#) means significance compared to EVs-FAPs CTR, $^{\#\#}P < 0.01$. § indicates significance by ANOVA test; $^{\S\S}P > 0.01$.

D Graph relative to Notch1 expression in MuSCs isolated from 1.5-month-old mdx mice treated with either vehicle (CTR) or TSA (TSA), and in EVs derived from FAPs (EVs-FAPs) isolated from 1.5-month-old mdx mice treated with either vehicle (CTR) or TSA (TSA) (n = 3). Star (*) indicates statistical analysis by Tukey's test relative to mdx vehicle-treated mdx mice (CTR); $^*P < 0.05$. § indicates significance by ANOVA test; $^{\S\S}P > 0.01$.

E Representative images showing myofibers cultured alone (CTR) or with extracellular vesicles isolated from FAPs (EVs-FAPs) and stained with PKH-67 (green) and MyoD (red). Nuclei were counterstained with DAPI (blue). Arrows represent nuclei positive for both PKH-67 and MyoD. Scale bar = 25 μm.

F From left to right: representative images of myofibers cultured for 24 h alone (–) or with conditioned media of FAPs that were previously exposed or not to TSA and GW4869 (MEDIA-FAPs) or extracellular vesicles (EVs-FAPs) collected from FAPs exposed or not to TSA *in vivo* (CTR and TSA) and transfected with antagomiR-206 (TSA A-206). Myofibers have been stained for EdU (cyan) and immunofluorescence with Pax7 (green) and MyoD (red). Nuclei were counterstained with DAPI (blue). (n = 3). Scale bar = 25 μm.

G Graph showing the average of nuclei positive for Pax7 (green) and MyoD (red) in the conditions indicated in (F). Star (*) indicates statistical analysis by Tukey's test relative to myofibers cultured alone (–), (n = 3, biological replicates). $^*P < 0.05$, $^{**}P < 0.01$; $^{***}P < 0.001$; $^{***}P < 0.0001$; hash (#) means significance compared to MEDIA-FAPs CTR, $^{\#}P < 0.05$; (†) means significance to EVs-FAPs CTR, $^{\dagger}P < 0.05$, while ¶ means significance compared to EVs-FAPs TSA, $^{¶¶¶¶}P < 0.0001$. § means significance by ANOVA test; $^{\S\S}P < 0.01$.

Data information: All data correspond to the average ± SEM.

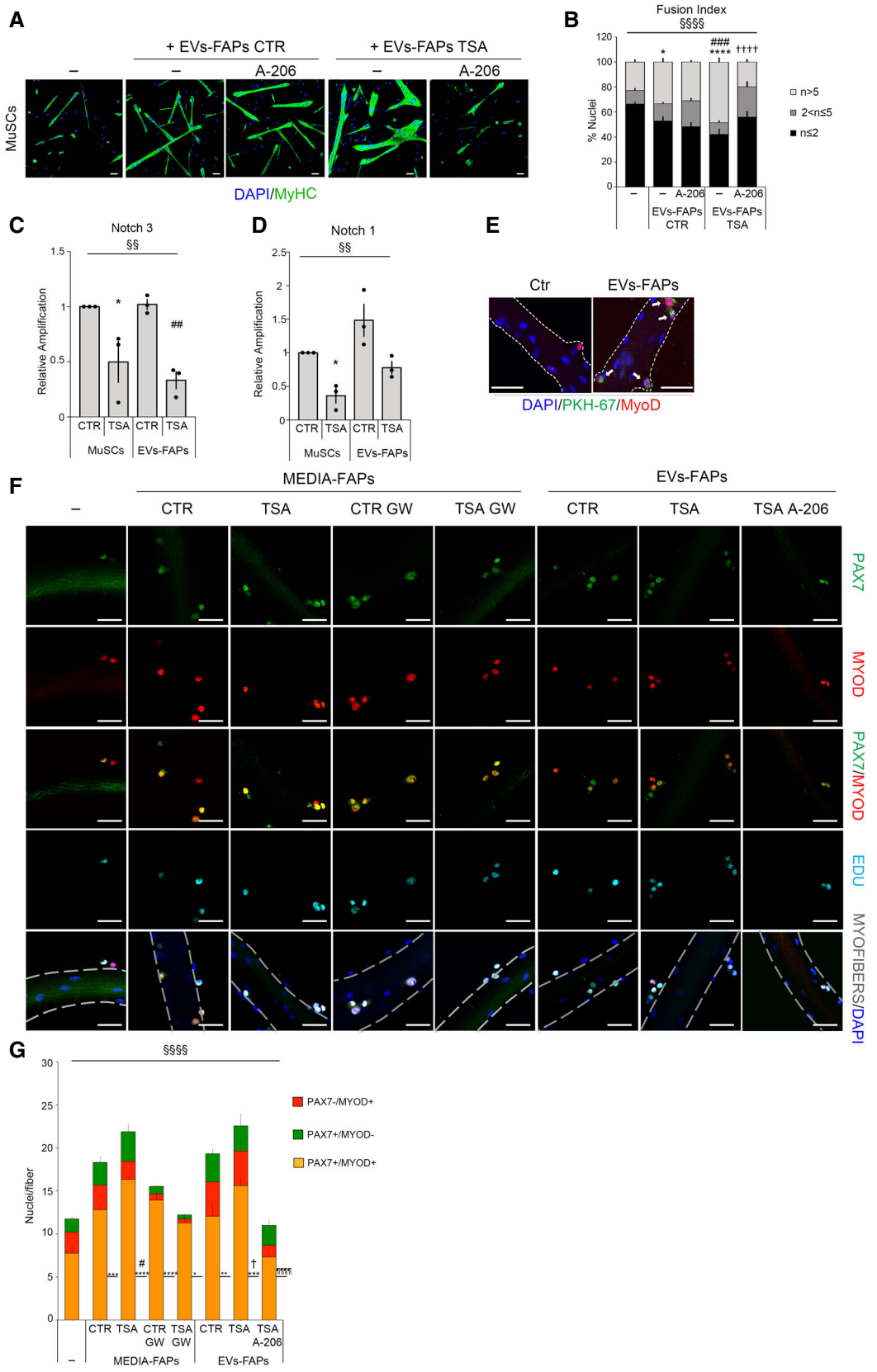
A
+ EVs-FAPs CTR
+ EVs-FAPs TSA
–
–
A-206
–
A-206
MuSCs
DAPI/MyHC
B
Fusion Index
§§§§
% Nuclei
n>5
2<n≤5
n≤2
EVs-FAPs CTR
EVs-FAPs TSA
C
Notch 3
§§
Relative Amplification
CTR TSA CTR TSA
MuSCs EVs-FAPs
D
Notch 1
§§
Relative Amplification
CTR TSA CTR TSA
MuSCs EVs-FAPs
E
Ctr
EVs-FAPs
DAPI/PKH-67/MyoD
F
MEDIA-FAPs
EVs-FAPs
–
CTR
TSA
CTR GW
TSA GW
CTR
TSA
TSA A-206
PAX7
MYOD
PAX7/MYOD
EDU
MYOFIBERS/DAPI
G
§§§§
Nuclei/fiber
PAX7-/MYOD+
PAX7+/MYOD-
PAX7+/MYOD+
CTR TSA CTR GW TSA GW CTR TSA TSA A-206
MEDIA-FAPs
EVs-FAPs

Figure 5.

fibrotic and adipose tissue that typically compromises contractile activity and regenerative potential of muscles.

While a variety of soluble factors, including inflammatory cytokines and growth factors, have been implicated as mediators of reciprocal functional interactions between the major cellular components of the muscle stem cell niche, EVs are emerging as powerful tool to transfer biochemical and genomic information from one cell type to another (Lee *et al*, 2012; Iraci *et al*, 2016; Kalluri & LeBleu, 2020). Indeed, by virtue of their content in proteins and nucleic acids, EVs enable the cross-activation of biological process between neighbor cells that account for their functional interactions. As such, the qualitative and quantitative control of proteins and RNA content appears as two major determinants of EV biological activity. Likewise, the direction of cell-to-cell transmission of EVs influences the final biological outcome of EV activity. Our finding that a subset of miRs up-regulated in EVs from FAPs of dystrophic muscles exposed to HDACi promote MuSC activity and compensatory regeneration of DMD muscles indicates that the biological activity of EVs is in principle pharmacologically tunable for therapeutic purposes.

A seminal discovery from Peterson's laboratory has recently revealed that MuSC-derived exosomes containing miR-206 are required to eliminate fibrosis during muscle hypertrophy (Fry *et al*, 2017). Moreover, myofiber-derived exosomes have been reported to promote skeletal myogenesis (Choi *et al*, 2016). The pro-regenerative and anti-fibrotic activities of miR-206 have been largely documented by previous studies (Ma *et al*, 2015). However, while these studies invariably indicated skeletal myofibers and MuSCs as only source of miR-206, our previous studies have revealed that FAPs from dystrophic muscles turn into an alternative cellular source of miR-206, once exposed to HDACi, and identified a miR-206-directed network that represses the adipogenic and fibrotic program in FAPs of dystrophic muscles (Saccone *et al*, 2014).

Our study provides the first evidence that FAP-derived EVs mediate functional interactions with MuSCs and that EV-miR content could be pharmacologically modified by epigenetic drugs (e.g., by HDACi) for therapeutic purposes in both human DMD patients and mouse model of DMD. In this regard, we note that the beneficial effects of focal delivery of EVs-FAPs TSA by i.m. injection were comparable or even greater than those observed upon systemic delivery of TSA (see Fig 4).

Our results further extend our knowledge on the role of miR-206 expressed in FAPs of DMD muscles exposed to HDACi (Saccone *et al*, 2014), by showing that it is incorporated into EVs, which are released in the regenerative environment and are uptaken by MuSCs. Our data show that mdx MuSCs that incorporated EVs released from HDACi-treated FAPs exhibited a fivefold increase in miR-206. In this regard, while the levels of miR-206 are significantly lower in FAPs and FAP-EVs, as compared to MuSCs, repeated uptake of large amounts of FAP-derived EVs overtime can lead to an overall increase in miR levels, as observed in MuSCs from DMD muscles exposed to HDACi. This is consistent with the very high numeric ratio between FAPs and MuSCs during muscle regeneration, whereby multiple FAPs can feed one MuSC. Furthermore, the output of EV release from FAPs could also account for repeated events of EV transfer from FAPs to MuSCs, to further increase the amount of miR that can be potentially be transferred from FAPs to MuSCs. We speculate that an increased exchange of EVs from FAPs to MuSCs could support the high regeneration demand imposed to MuSCs of DMD muscles subjected to repeated cycles of degeneration/regeneration. In this condition, pharmacological modulation of EV content (as obtained by exposure to HDACi) could exert potent biological effects, as observed in our study.

Although we have detected a low percentage of MuSCs (2%) that incorporated FAP-derived EVs upon intramuscular injection, we argue that this low number might underestimate the actual rate of EV incorporation by MuSCs in DMD muscles, due to the progressive dilution of the EV tracing signal (e.g., PKH-67) upon mitotic division and/or differentiation into myofibers of MuSCs—two events that occur at high frequency at early stages of DMD progression. While these scenarios remain purely speculative at this stage, the advent of more accurate methods of EV tracing in recipient cells will allow to clarify this important issue in future studies.

Based on our data, we propose that additional amounts of miR-206 levels provided by EVs from HDACi-treated FAPs might correct the dysfunctional phenotype of MuSCs from DMD muscles. The recent finding that dystrophin-deficient MuSCs lose their ability to divide asymmetrically and regenerate DMD muscles (Dumont *et al*, 2015a; Chang *et al*, 2016) indicates that additional events downstream of dystrophin can be dysregulated in DMD MuSCs. Among them, repression of miR-206 expression has been previously reported in DMD MuSCs (Cacchiarelli *et al*, 2010) and could be compensated by FAP-derived EVs-miR-206 in order to restore MuSC ability to regenerate dystrophic muscles.

Seemingly, conflicting data have been reported regarding the role of miR-206 in the pathogenesis of DMD, with beneficial effects observed in mdx mice upon transgenic miR-206 overexpression (Liu *et al*, 2012), while genetic ablation of the miR-206/133b cluster could not worsen the pathology in mdx mice (Boettger *et al*, 2014). These data indicate that although miR-206 is dispensable for the compensatory regeneration observed in mdx mice, increased amounts of intramuscular miR-206 might exert therapeutic effects by enhancing the regeneration potential of mdx muscles.

Of note, a multitude of miRs, in addition to miR-206, were found to be up-regulated in EVs derived from DMD FAPs, upon the exposure to HDACi, and antagomiR-mediated neutralization of one of these additional miR (e.g., miR-145) indicates that the cooperative action of these miRs accounts for the net biological effect of EVs from HDACi-treated DMD FAPs. Further studies should elucidate the mechanism by which HDACi regulates EV biogenesis and content, both the transcriptional and post-transcriptional levels, and will define the potential for further development of interventions based on FAP-derived extracellular vesicles as potential selective treatment for DMD.

Finally, our study suggests that specific interstitial amount of intra-EV miRs (i.e., miR-206) could be exploited as biomarker of disease progression and/or therapeutic response to interventions that counter DMD progression.

Materials and Methods

Experimental model and subject details

Animals

Mice were bred, handled, and maintained according to the standard animal facility procedures, and all experimental protocols were approved by the internal Animal Research Ethical Committee

according to the Italian Ministry of Health and the ethic committee of the Fondazione Santa Lucia (FSL) approved protocols.

C57BL/6 mice were provided by the Core Structure of the EMMA (European *Mouse* Mutant Archive, Monterotondo, Rome); C57BL/6 mdx mice were purchased from Jackson Laboratories. Note that the term of "young" is referred to C57BL/6/mdx mice of 6/8 weeks old, which includes the temporal frame in which the beneficial effects of HDACi are restricted (Mozzetta *et al*, 2013; Saccone *et al*, 2014), while the term of "old" is referred to C57BL/6/mdx mice of 1 year old.

Human samples

Human biopsies were collected with informed patients' and parental consent in compliance with Good Clinical Practice and the Declaration of Helsinki and provided by Dr. Bertini and Dr. D'Amico (Ospedale Bambino Gesù, Rome). We used 10-μm transversal sections isolated for research purposes from vastus medialis of DMD boys, at different ages: 1 year old ($n = 2$), 4 years old ($n = 3$), and 9 years old ($n = 2$), and we compared with a vastus medialis section of control (non-DMD) samples.

Human bioptic samples obtained from brachial biceps from DMD boys participating to the clinical trial with Giv (www.ClinicalTrials.gov; EudraCT Number: 2012-002566-12; Sponsor Protocol Number: DSC/11/2357/43) were provided by Italfarmaco S.p.A. (Milan) (23). The phase II study was approved by the local ethics committees and authorized by the Competent Authority of Italy. Parents of the participants provided informed written consent and each subject provided written assent before participation.

Mice and animal procedures

Animals were used at the specified age and treated with daily intraperitoneal injections of Trichostatin A (TSA) (0.6 mg/kg/day for 15 days to obtain FAPs for co-culture and for EV isolation or 21 days for the transplant experiments; #T8552, Sigma) and dissolved in DMSO solution or in DMSO alone as vehicle control (CTR). Muscle injury was performed by intramuscular injection in tibialis anterior (TA) of Cardiotoxin (CTX) (10 μM, 10 mg/ml) (#L8102, Latoxan Valence, France, http://latoxan.com), 4 days before mouse sacrifice.

FAP-derived EVs at a final concentration of 10 μg in 20 μl of PBS 1× (0.5 μg/μl) (#14190-1444, Gibco by Life Technologies) and its vehicle of control (20 μl PBS 1×) were injected 3 times in left TA of young C57BL/6/mdx mice: every 7 for 21 days.

Histology and *in situ* hybridization

The tibialis anterior muscles were snap-frozen in liquid nitrogen-cooled isopentane and then cut transversally with a thickness of 7 μm.

For Masson's trichrome staining to analyze fibrotic tissue, muscle cryo-sections were fixed for 20′ at 56°C in Bouin's solution (#HT10132, Sigma) and then stained in Working Weigert's Iron Hematoxylin solution for 5 min (#HT1079, Sigma), washed in running tap water for 5 min, and stained in Biebrich scarlet-acid fuchsin for 5 min (#HT151, Sigma). Sections were rinsed in deionized water and re-fixed in freshly made phosphomolybdic/phosphotungstic/dH_2O (1:1:2) acid solution for 8 min (#HT153, #HT152, Sigma), and then, they were stained in Aniline Blue solution for 5 min (#HT154, Sigma) and in acetic acid 1% for 2 min (#27221, Sigma). The slides were dehydrated in ethanol (#02860, Sigma) and xylene (#X1040, Sigma) and mounted with EUKITT (#03989, Sigma), and then visualized using a Nikon Eclipse 90i; collagen fibers are stained in blue, the nuclei are stained in black, and the muscle tissue is stained in red. miRNA *in situ* hybridization was performed in formaldehyde- and carbodiimide (EDC)-fixed TA cryo-sections (0.16 M 90 min at RT, #25952-53-8, Merck KGaA). After washing with 0.2% glycine (#G8898, Sigma) and TBS, cryo-sections were acetylated using 0.1 M triethanolamine and 0.25% acetic anhydride for 25 min at RT (respectively, #90275, #A6404, Sigma). These steps are followed by a pre-hybridization using 2× SSC, 25% formamide (#F9037, Sigma), and 0.2% Triton (#X100, Sigma) for 30 min at RT, and by the overnight hybridization at 4°C with the hsa-miR-206 probe (10 pmol, #18100-01, Exiqon) dissolved in a solution of 50% formamide, 250 μg/ml tRNA (#R1753, Sigma), 200 μg/ml SSDNA (#D7656, Sigma), 10% dextran sulfate (#D8906, Sigma), and 2× SSC. The hybridization was followed by specific washes with SSC to eliminate non-specific binding of probe (5× SSC 5 min at RT, 1× SSC 15 min at 45°C, 2% BSA in 0.2× SSC 15 min at 4°C, 2× SSC 5 min at RT, TN buffer 10 min at RT, and TNT buffer 15′ at RT) and by the incubation of cryo-section using anti-digoxigenin-ap Fab fragments (1/100, #11093274910, Roche) dissolved in TN buffer for 2 h at RT. To reveal the miRNA probe-specific binding, cryo-sections, covered from light, were incubating overnight at 4°C with 0.375 mg/ml of NBT and 0.188 mg/ml BCIP dissolved in a solution of TMN buffer (respectively, #11383213001 and #11383221001, Roche).

TN buffer is composed of 0.1 M Tris–HCl (#T1503, Sigma) and 0.15 M NaCl (#S3014, Sigma) at pH 7.5; TNT buffer is TN buffer with 0.1% Tween (#P1379, Sigma), while TMN buffer is composed of 0.1 M Tris–HCl, 0.005M $MgCl_2$ (#M8366, Sigma), 0.5 M NaCl, and 2 mM of Levamisole (#L9756, Sigma).

Isolation of FAPs and satellite cells (MuSCs)

hMuSCs were isolated from human biopsies as CD31 ^{neg}/CD45 ^{neg}/CD11b ^{neg} (Lin-)/CD56 ^{pos} cells and ehFAPs as Lin-/CD56 ^{neg} cells. Live/dead staining was used to check cell vitality.

FAP cells were isolated from mdx mice as TER119^{neg}/CD45^{neg}/CD31^{neg}/alpha7INTEGRIN^{neg}/SCA-1^{pos} cells; MuSCs were isolated from mdx mice as TER119^{neg}/CD45^{neg}/CD31^{neg}/alpha7INTEGRIN^{pos}/SCA-1^{neg} cells (Mozzetta *et al*, 2013).

Briefly, human biopsies or hind limb muscles for each mouse were minced and put into a 15-ml tube containing 4 ml of HBSS (#24020-091, Gibco), BSA (0.2%, #A7030, Sigma), and 10 units/ml penicillin and 10 μg/ml streptomycin (P/S), 2 mg/ml collagenase A (#10103586001, Roche), 2.4 U/ml dispase II (#04942078001, Roche), and 10 mg/ml DNase I (#11284932001, Roche) at 37°C under gentle agitation for 1 h and 30 min. The supernatants were filtered through a 100-μm, 70-μm, and 40-μm cell strainers (#08-771-19, #08-771-2, #08-771-1, BD Falcon). Cells were spun for 15 min at 300 *g* at 4°C; the pellets were resuspended in 0.5 ml of HBSS 1× containing DNase I and incubated with antibodies on ice for 30 min. The following antibodies were used: CD45-eFluor 450 (1/50, #48-0451-82, leukocyte common antigen, Ly-5, eBioscience), CD31-eFluor 450 (1/50, PECAM-1, #48-0311-82, eBioscience),

TER-119-eFluor 450 (1/50, clone TER-119, #48-5921-82, eBioscience), Sca1-FITC (1/50, Ly-6A/E FITC, clone D7, #11-5981-82, eBioscience), Itga7-649 (1/500, AbLab #67-0010-01), anti-human CD31-FITC (#21270313, ImmunoTools), anti-human CD45-FITC (#130-080-202, Miltenyi Biotec), anti-human CD11b-FITC (#130-081-201, Miltenyi Biotec), and anti-human CD56-PE (#12-0567-42, eBioscience). HBSS was added, and cells were spun for 5 min at 300 *g* at 4°C to stop the reaction. The cells were resuspended in HBSS containing 1% DNase I and were isolated based on size, granulosity, and fluorophore levels using a FACS MoFlo Astrios EQ High Speed Cell Sorter (Beckman Coulter) and analyzed using FlowJo.

Cell culture

MuSCs and FAPs, either from human or mouse samples, were cultured after sorting directly in culture media: for MuSCs: 20% FBS (#16000044, Gibco), 10% HS (#26050-070, Gibco), 1% penicillin–streptomycin (#15140, Gibco), 1% Chicken Embryo Extract (CEE, #CE-650-F, Seralab) in DMEM + Pyruvate (#41966, Gibco), and for FAPs: BIO-AMF-2 (Biological Industries). MuSCs were plated at low density on regular cell culture dishes coated with gelatin 0.1% (#07903, Stemcell).

FAP cells were cultured in BIO-AMF-2 at high density (200,000 cells in 10-cm-well plate) for extracellular vesicle isolation and at low density (40,000 or 10,000 cells, respectively, in 6- or 24-well dishes) for co-culture experiments.

For HDACi *in vitro* treatment, cells were exposed to TSA (50 nM) for 12 h before EV isolation.

To isolate EVs, cells reached 80–90% of confluence; then, the medium was replaced with serum-free DMEM (+ pyruvate + 4.5 g/l glucose + glutamate) for 24 h.

Transwell co-culture experiments

MuSCs and FAP cells, both from human or mouse samples, were co-cultured by using inserts with 1.0-μm porous membrane (#353102, #353104, Falcon) to avoid direct contact between populations.

Freshly sorted MuSCs were plated in the bottom of the plate, while FAP cells were plated on the upper insert.

Single-fiber isolation and culture

Single fibers were isolated from tibialis anterior, extensor digitorum longus, gastrocnemius, and soleus muscles of C57BL/6J-WT mice (Tucciarone *et al*, 2018) and cultured in proliferating medium (GM1: DMEM + pyruvate + 4.5 g/l glucose + glutamate, 10% horse serum (HS), 0.5% Chicken Embryo Extract) for 24 h, and then exposed for the next 24 h to GM1 conditioned media derived from culture of FAPs (MEDIA-FAPs) isolated from young mdx mouse treated for 15 days with vehicle (CTR) or mdx mice treated with TSA (TSA) or media isolated from FAPs CTR and TSA pre-treated with the GW4869 to inhibit exosome biogenesis. In a parallel, independent experiment, single fibers were exposed to EVs (EVs-FAPs) purified from MEDIA-FAPs and added to GM1 for 24 h.

Cell treatments

The transfection of FAPs with pCT-CD63-GFP plasmid (#CYTO120-PA-1, System Biosciences) and with a GFP-control vector (mock) in cell culture inserts was accomplished using Lipofectamine 2000 (#12566014, Thermo Fisher Scientific) 6 h before MuSC co-culture. Transwell co-cultures were maintained in GM2 medium for 24 h and then harvested for GFP analyses.

To decrease FAP-EV release, GW4869 (10 μM, #D1692, Sigma) was added to FAP culture 30 min before the co-culture setting with MuSCs. To wash away any residual trace of GW4869, FAP media was refreshed right before co-culture.

For siRNA or antagomiR transfection, FAPs isolated from mdx mice were transfected with siRNA for Drosha, antagomiR-206 (mmu-miR-206-3p miRCURY LNA™ microRNA inhibitor, Exiqon), and antagomiR-145 (mmu-miR-145a-5p miRCURY LNA™ microRNA inhibitor, Exiqon) using DharmaFECT 3.0 (#T2003-03, Thermo Fisher Scientific) according to the manufacturer's instructions; after 6 h, the medium was replaced with DMEM serum-free for 24 h before exosome isolation and purification.

To stain FAP-derived EVs, FAP cells were incubated with the lipidic dye PKH-67 (#P7333, Sigma) according to the manufacturer's instructions prior to transwell co-culture with MuSCs.

In *ex vivo* experiments, FAP-derived EVs (10 μg) isolated by TEIR were put in culture with MuSCs or with myofibers in the cell culture media.

For the *in vitro* treatment with TSA, cells were exposed to TSA (50 nM) for 12 h.

Immunofluorescence

For immunofluorescence analysis, cryo-sections and cells were fixed in 4% PFA for 10 min and permeabilized with 100% cold acetone (#32201, Sigma) for 6 min at −20°C or 100% cold methanol (#32213, Sigma) for 6 min at −20° or with 0.25% Triton for 15 min at RT. Muscle sections were blocked for 1 h with a solution containing 4% BSA (#A7030, Sigma) in PBS. The primary antibody incubation was performed O.N. at 4°C, and then, the antibody binding specificity was revealed using secondary antibodies coupled to Alexa Fluor 488, 594, or 647 (Invitrogen). Sections were incubated with DAPI in PBS for 5 min for nuclear staining, washed in PBS, and mounted with glycerol 3:1 in PBS. The primary antibodies used for immunofluorescences are as follows: rabbit anti-Laminin (1/400, #L9393, Sigma); rat anti-SCA1 (1/100, #11-5981-82 Ly-6A/E FITC, eBioscience); mouse anti-eMyHC (1/20, #F1.652, Developmental Studies Hybridoma Bank, DSHB, http://dshb.biology.uiowa.edu/F1-652); mouse anti-MF20 (1:20, Developmental Studies Hybridoma Bank, DSHB, http://dshb.biology.uiowa.edu/MF-20); mouse anti-PAX7 (1/10, Developmental Studies Hybridoma Bank, DSHB, http://dshb.biology.uiowa.edu/PAX7); rabbit anti-MyoD-318 (#SC760, Santa Cruz Biotechnology); EDU (#C10350, Invitrogen); rat anti-CD63 PE (#143904, clone NUG-2, BioLegend) and myeloperoxidase/MPO (1/100 #MAB3174, R&D), and anti-human C90 (Thy-1) (1:150 #14090980, eBioscience).

Cytohistochemistry

To stain lipids in ehFAPS, cells were fixed in 4% PFA for 10 min and then washed with 60% isopropanol, stained with Oil Red O in 60% isopropanol, and rinsed with water (Mozzetta *et al*, 2013).

RNA preparation and RT–qPCR

Total RNA from cell cultures and from plasma was extracted with TRIzol reagent (#T9424, Sigma), and 0.5–1 μg was retro-transcribed

using the TaqMan reverse transcription kit (Applied Biosystems). Real-time qPCR was performed using primers (MmDrosha Fw:5′ TGCAAGGCAATACGTGTCATAG 3′; MmDrosha Rev:5′ TGAAAGC TGGTGCTGAAGGT 3′; MmNotch1 Fw: 5′TGAGACTGCCAAAG TGTTGC 3′; MmNotch1 Rev: 5′ GTGGGAGACAGAGTGGGTGT 3′; MmNotch3 Fw:5′ GTCCAGAGGCCAAGAGACTG 3′; MmNotch3 Rev:5′ CAGAAGGAGGCCAGCATAAG 3′; MmCol1a1 Fw:5′ CCT CAGGGTATTGCTGGACA 3′; MmCol1a1 Rev: 5′ GAAGGACCT TGTTTGCCAGG 3′; MmCol3a1 Fw:5′ CCCAACCCAGAGATCCCATT 3′; MmCol3a1 Rev:5′ GGTCACCATTTCTCCCAGGA 3′; MmFibronectin Fw:5′ TCCACGCCATTCCTGCGCC 3′ MmFibronectin Rev: 5′ GCACCCGGTAGCCAGTGAG 3′).

EVs

EVs isolation

EVs were isolated from FAP serum-free cell culture medium in parallel by ultracentrifugation (UC) and with Total Exosome Isolation Reagent (TEIR) (#4478359, Invitrogen by Thermo Fisher Scientific) according to the manufacturer's instructions. EVs were isolated by UC and quantified according to a previously published method (Théry *et al*, 2006; Van Deun *et al*, 2014). This isolation method included a penultimate centrifugation step in Eppendorf polypropylene conical tubes (10,000 *g* for 30 min at 4°C, in Eppendorf rotor F-34-6-38) that allowed the removal/isolation of larger microvesicles. Subsequently, nano-sized EVs, comprised mainly of exosomes, were pelleted in Beckman Coulter polypropylene open top tubes (110,000 *g* for 70 min at 4°C, in Beckman rotor SW28). After washing, the pellet was resuspended either in RIPA buffer or in PBS, for further immunoblotting or biophysics and molecular analyses, respectively. To estimate the amount of secreted vesicles, we quantified and compared the total protein content of the vesicle lysates using the BCA assay.

EVs were purified from tibialis anterior gently dissociated in serum-free DMEM (24 h). Cell debris and organelles were eliminated by centrifugation at 2,000 *g* for 20 min, and EVs were isolated using TEIR. For their characterization by electron microscopy, EVs were isolated using TEIR and then purified using exosome spin columns (MW3000, Invitrogen) following the manufacturer's protocol.

EVs characterization

EV size distribution was determined by dynamic light scattering (DLS) measurements. Collected EV samples were diluted to a final concentration of 15 μg/ml total protein content in order to avoid multiple scattering artifacts. Static and dynamic light scattering measurements were performed at 20°C by using a Brookhaven Instruments BI-9000 correlator and a solid-state laser tuned at $\lambda_0 = 532$ nm. Scattered intensity autocorrelation functions *g2(t)* have been analyzed by using multiple gamma functions for the diffusion coefficient and therefore by using the classic Stokes–Einstein relation to determine the size distribution P(D) of vesicles, where the size parameter D is actually the hydrodynamic radius of diffusing vesicles (Noto *et al*, 2012).

EV morphology was examined for scanning electron microscopy analysis. EVs isolated and purified from FAPs by TEIR were fixed in 4% (v/v) paraformaldehyde, dehydrated by a series of incubations in 30, 50, and 70% (v/v) ethanol, and dried on aluminum support for SEM. EVs isolated were coated with gold. A SEM LEO 1450VP (Carl Zeiss Meditec, Oberkochen, Germany) was employed to acquire backscattered electron images using 20 keV electrons leading to an information depth of about 1.5 μm. Images with a scan size of 30 × 30 μm were acquired, at a resolution of 1,024 × 1,024 pixels.

EVs labeling

Acridine orange

To detect nucleic acid content, FAP-derived EVs (10 μg) isolated by TEIR were labeled with acridine orange (AO) (#235474, Sigma) (0.1 μg/ml) for 30 min at room temperature and added to MuSCs in order to reveal by immunofluorescence the RNA exchanged from FAPs to MuSCs.

Pkh-67

To visualize EVs, FAP-derived EVs (10 μg) are stained for 5 min at room temperature RT with 0.5 μl of PKH67 Green Fluorescent Cell Linker Kit for General Cell Membrane Labeling (#P7333, Sigma) and then polished with the exosome spin columns (#4484449, Invitrogen by Thermo Fisher Scientific) following the manufacturer's protocol. The stained EVs are detected by immunofluorescence into myofibers and by cyto-fluorimetric analysis in mouse muscle after their *in vivo* injection.

Flow cytometric analysis of extracellular vesicles released by FAPs

EVs purified from FAPs isolated from mdx mice and treated with DMSO (CTR) and TSA (50 nM) were stained with PKH67 dye and acquired on the CytoFLEX flow cytometer (Beckman Coulter, Brea, CA, USA). The cytometer was calibrated using a mixture of non-fluorescent silica beads and fluorescent (green) latex beads (Apogee, UK) with sizes ranging from 110 to 1,300 nm. This calibration step enabled the determination of the sensitivity and resolution of the flow cytometer (fluorescent latex beads) and the size of extracellular vesicles (silica beads) (Logozzi *et al*, 2017). All samples were acquired at low flow rate for the same amount of time (1 min) in order to obtain an estimate of absolute counts of microvesicles comparable between various samples. The analysis of the data was performed with FlowJo software (FlowJo, LLC; Ashland, Oregon, USA). The FAPs were purified by FACS and seeded under the same condition and in the same number for all the samples analyzed. For EV isolation and labeling, all the samples were treated in the same way.

EV content

Protein

EVs isolated were lysed for protein extraction in RIPA buffer (50 mM Tris–HCl, pH 7.4; 150 mM NaCl; 1% NP-40; protease inhibitors). The total extravesicular protein content was quantified using the micro bicinchoninic acid protein assay (BCA) (#23235, Thermo Fisher Scientific).

Western blot

Western blot was performed on 12 ug of total lysate (WCL) and of EV proteins using antibodies against the following proteins: rabbit anti-CD63 (1/300, H-193, Santa Cruz Biotechnology), mouse anti-Hsp70 (1/2,500, clone BRM-22, Sigma-Aldrich), rabbit anti-Calnexin (CANX) (1/1,000, NB100-1965, Novus Biologicals), rabbit anti-Flotillin-1 (1/200, H-104, Santa Cruz Biotechnology), mouse anti-Alix (3A9) (1/500, Cell Signaling Technologies #2171), and mouse

monoclonal Col3a1 (B-10) (1/150, Santa Cruz Biotechnologies, #sc-271249).

As total lysate normalization, we used Ponceau quantification.

microRNA

Total extravesicular RNA was extracted with Total Exosome RNA Protein Isolation Kit (#4478545, Thermo Fisher Scientific). TaqMan MicroRNA Assays were performed according to the manufacturer's recommended protocols (Applied Biosystems). The threshold cycle (Ct) was defined as the fractional cycle number at which the fluorescence passes the fixed threshold. U6 snRNA served as an endogenous control for normalization.

In particular, total EVs-RNA was retro-transcribed using TaqMan MicroRNA Reverse Transcription Kit (#4366596, Thermo Fisher Scientific).

For greater sensitivity, the cDNA was pre-amplified using TaqMan PREAMP Master Mix (#4391128, Thermo Fisher Scientific) and Megaplex PreAMP Primers and then amplified using high-multiplexed Megaplex Primer Pool (#4444766, Thermo Fisher Scientific) and the TaqMan 2× Universal Master Mix II (#4440040, Thermo Fisher Scientific) on TaqMan Rodent MicroRNA A/B Cards Array version 3.0 (#4444909, Thermo Fisher Scientific).

qRT–PCR

For microRNA validation, total EVs-RNA was extracted with Total Exosome RNA Protein Isolation Kit (#4478545, Invitrogen by Thermo Fisher Scientific) and was retro-transcribed using the Qiagen Reverse Transcription Kit (miScript II RT Kit, #218161, Qiagen) and pre-amplified using miScript PreAMP PCR Kit (#331451, Qiagen).

Real-time qPCR was performed using miScript SYBR Green PCR Kit (#218073, Qiagen) and using primers reported in Table 1. All the conditions are provided in the manufacturer's protocol.

FAP-derived EV intramuscular injection

FAP-derived EVs at a final concentration of 10 μg in 20 μl of PBS 1× (0.5 μg/μl) were injected 3 times in left tibialis anterior (TA) of C57BL/6/mdx mice: every 7 days for 21 days. The right TA was injected with vehicle (20 μl PBS 1×) following the same timing described for EV injection.

RNA sequencing

For RNA-sequencing sample preparation, MuSCs and FAPs were freshly isolated by FACS from 6 C57BL/6 mdx male mice of 8 weeks old treated or not with TSA for 15 days. RNA was collected using TRIzol reagent (#T9424, Sigma). About 100 ng/μl of total RNA was sent in duplicate to IGA (Istituto di Genomica Applicata, Udine) for RNA sequencing using Illumina TruSeq Stranded Total RNA Kit Ribo-Zero GOLD on Illumina HiSeq 2500 platform.

Table 1. List of microRNA oligos purchased by Qiagen and used in the current work.

MS00033740	Qiagen	Hs_RNU6-2_1
MS00001372	Qiagen	Mm_miR-29a_1
MS00033761	Qiagen	Mm_miR-494_2
MS00011704	Qiagen	Mm_miR-30a_1
MS00002387	Qiagen	Mm_miR-449_1
MS00001869	Qiagen	Mm_miR-206_1
YCO0073796	Qiagen	Mm_miR-145a-5p

Statistical analysis

The number of independent experimental replications and precision measures are reported in the figure legends (n, mean ± SEM). Statistical analysis was performed using Prism 7.0 A software (Pad Software).

Most of the data meet the assumptions of the tests (e.g., normal distribution). Whether data do not meet the assumptions of the tests (e.g., normal distribution), Mann–Whitney's test was used as non-parametric test. For the assumption of normality, we used Shapiro–Wilk normality test; unpaired, two-tailed Student's t-test was used to compare the means of two groups; and Welch's correction was applied to account for unequal variances, while one-way analysis of variance (ANOVA) was used for comparison among the different groups, while two-way analysis of variance was used for comparison among different groups to examine the influence of different independent variables on dependent variable. When ANOVA was significant, post hoc testing of differences between groups was performed using Tukey's honestly significant difference (HSD). A $P < 0.05$ was considered statistically significant.

For animal studies, the sample size was calculated by power analysis. The animal experiments were not randomized. The investigators were not blinded to allocation during experiments and outcome assessment. No exclusion criteria were applied to exclude samples or animals from analysis.

Data acquisition, analysis, and quantification

The cells positive for the stainings described in the text were quantified using ImageJ software (https://imagej.nih.gov/ij/download.html). The cross-sectional area (CSA) was also calculated using the ImageJ software and Macro seg 5 modif.ijm specific plugin. Fibrotic areas were measured from sections evaluating image analysis algorithms for color deconvolution. ImageJ was used for image processing, the original image was segmented with three clusters, and the plugin assumes images generated by color subtraction (white representing background, blue collagen, and magenta non-collagen regions).

FACS profile analysis of MuSCs and FAPs was performed using FlowJo software (https://www.flowjo.com).

RNA-seq

The RNA-sequencing analysis was performed mapping more than 20 millions of reads for each sample to the Mus Musculus GRCm38.78 genome using TopHat 2.0.9. Read count was performed with HTSeq-0.6.1p1. Mapped reads were analyzed with RStudio using DESeq2 to obtain normalized RPKM, P-value, P-adjusted, and log2 fold change values. Genes were considered differentially expressed if the P-adjusted value was < 0.1.

Additional raw data that support the findings of this study are available from the corresponding authors upon reasonable request. RNA-seq data are available through SRA accession code SRP143532 (Iannotti *et al*, 2018).

miRNA's targets analysis

miRNA pathway analysis was performed using miRPath based on predicted miRNA targets provided by the DIANA-microT-CDS algorithm and/or experimentally validated miRNA interactions derived from DIANA-TarBase v6.0 (http://www.microrna.gr/miRPathv2).

Prediction of miRNA-mRNA interactions and network construction

Data from RNA-seq ($P_{adj} < 0.1$) in MuSCs (treated or not with TSA) and microarray analysis in FAP (treated or not with TSA)-derived EVs were uploaded in IPA (https://www.qiagenbioinformatics.com/products/ingenuity-pathway-analysis/). With the IPA tool "miR Target Filter", the miRNA up-regulated in FAPs-EVs was intersected with transcripts down-regulated in MuSCs after TSA treatment. Only interactions experimentally observed and highly predicted were selected for downstream analysis. *Notch* pathway was extrapolated from IPA database using the tool "grow", while its modulation was predicted by the Molecular Activity Predictor (MAP) tool. The cartoon was realized with IPA Path Designer.

Data availability

No new primary datasets have been generated and deposited in this study.

Expanded View for this article is available online.

Acknowledgements

We thank Dr Roberts and all members of Puri laboratory for reading the manuscript and for their insightful inputs. We thank them for critical discussion and daily support; we are grateful for precious comments during the experiments and manuscript preparation. We thank Dr. Mauro Manno —Institute of Biophysics (IBF), National Research Council (CNR) of Italy, Palermo, Italy, for DLS assay. We thank Giovanna Borsellino and Luca Battistini (Fondazione Santa Lucia, Roma, Italy) for isolation of MuSCs and FAPs by cell sorter. This work has been supported by the following funding: Association Francaise contre les Myopathies, Italian Ministry of Health (GR-2016-02362451) to V.S.; NIH/NIAMS 1R01AR076247-01, NIH/NIGMS R01 GM134712-01, MDA, and EPIGEN F7 to P.L.P.; DPP_Netherland postdoc fellowship to V.S.; DPP_Ita PhD fellowship to L.T., and AFM postdoc fellowship to S.C.

Author contributions

VS and MSa performed most of the experimental work and contributed to experimental design, data analysis, and discussions. In particular, MSa performed the *in vivo* experiments, stainings on human, and animal muscle sections. LT performed muscle fiber isolation and culture with FAP-derived EVs. MSc performed SEM analysis. VB and AB contributed experimentally to EV characterization. MDB performed FACS sorting experiments, and DFA contributed to CytoFLEX analysis of intramuscular-injected EVs. SCo and LT performed bioinformatics data analysis. ADA and ESB. provided human biopsies of control and DMD patients. SCa and PB were the sponsors of the clinical trial. MB contributed as collaborator for the research activity planning and as mentorship external to the core team. MSa, SCo, VS, and PLP conceived the experiments, supervised the study, and interpreted the data. PLP wrote the manuscript, and all authors discussed the results and commented on the manuscript.

Conflict of interest

VS, MS, and SC own shares of Exofix, a startup company that aims to develop exosome-based therapies. VS, MS, and SC are also co-inventors on a patent application filed by Exofix claiming exosome-based therapeutics.

References

Amirouche A, Tadesse H, Miura P, Bélanger G, Lunde JA, Côté J, Jasmin BJ (2014) Converging pathways involving microRNA-206 and the RNA-binding protein KSRP control post-transcriptionally utrophin A expression in skeletal muscle. *Nucleic Acids Res* 42: 3982 – 3997

Aswad H, Forterre A, Wiklander OPB, Vial G, Danty-Berger E, Jalabert A, Lamazière A, Meugnier E, Pesenti S, Ott C *et al* (2014) Exosomes participate in the alteration of muscle homeostasis during lipid-induced insulin resistance in mice. *Diabetologia* 57: 2155 – 2164

Bentzinger CF, Wang YX, Dumont NA, Rudnicki MA (2013) Cellular dynamics in the muscle satellite cell niche. *EMBO Rep* 14: 1062 – 1072

Bettica P, Petrini S, D'Oria V, D'Amico A, Catteruccia M, Pane M, Sivo S, Magri F, Brajkovic S, Messina S *et al* (2016) Histological effects of givinostat in boys with Duchenne muscular dystrophy. *Neuromuscul Disord* 26: 643 – 649

Blau HM, Cosgrove BD, Ho ATV (2015) The central role of muscle stem cells in regenerative failure with aging. *Nat Med* 21: 854 – 862

Boettger T, Wüst S, Nolte H, Braun T (2014) The miR-206/133b cluster is dispensable for development, survival and regeneration of skeletal muscle. *Skelet Muscle* 4: 23

Cacchiarelli D, Martone J, Girardi E, Cesana M, Incitti T, Morlando M, Nicoletti C, Santini T, Sthandier O, Barberi L *et al* (2010) MicroRNAs involved in molecular circuitries relevant for the Duchenne muscular dystrophy pathogenesis are controlled by the dystrophin/nNOS pathway. *Cell Metab* 12: 341 – 351

Chang NC, Chevalier FP, Rudnicki MA (2016) Satellite cells in muscular dystrophy - lost in polarity. *Trends Mol Med* 22: 479 – 496

Chen J-F, Tao Y, Li J, Deng Z, Yan Z, Xiao X, Wang D-Z (2010) microRNA-1 and microRNA-206 regulate skeletal muscle satellite cell proliferation and differentiation by repressing Pax7. *J Cell Biol* 190: 867 – 879

Choi JS, Yoon HI, Lee KS, Choi YC, Yang SH, Kim I-S, Cho YW (2016) Exosomes from differentiating human skeletal muscle cells trigger myogenesis of stem cells and provide biochemical cues for skeletal muscle regeneration. *J Control Release Off J Control Release Soc* 222: 107 – 115

Collino F, Deregibus MC, Bruno S, Sterpone L, Aghemo G, Viltono L, Tetta C, Camussi G (2010) Microvesicles derived from adult human bone marrow and tissue specific mesenchymal stem cells shuttle selected pattern of miRNAs. *PLoS ONE* 5: e11803

Colussi C, Mozzetta C, Gurtner A, Illi B, Rosati J, Straino S, Ragone G, Pescatori M, Zaccagnini G, Antonini A *et al* (2008) HDAC2 blockade by nitric oxide and histone deacetylase inhibitors reveals a common target in Duchenne muscular dystrophy treatment. *Proc Natl Acad Sci USA* 105: 19183 – 19187

Consalvi S, Saccone V, Giordani L, Minetti G, Mozzetta C, Puri PL (2011) Histone deacetylase inhibitors in the treatment of muscular dystrophies: epigenetic drugs for genetic diseases. *Mol Med* 17: 457 – 465

Consalvi S, Mozzetta C, Bettica P, Germani M, Fiorentini F, Del Bene F, Rocchetti M, Leoni F, Monzani V, Mascagni P *et al* (2013) Preclinical studies in the mdx mouse model of duchenne muscular dystrophy with the histone deacetylase inhibitor givinostat. *Mol Med* 19: 79 – 87

Consalvi S, Saccone V, Mozzetta C (2014) Histone deacetylase inhibitors: a potential epigenetic treatment for Duchenne muscular dystrophy. *Epigenomics* 6: 547 – 560

Consalvi C, Sandona M, Saccone V (2016) Epigenetic reprogramming of muscle progenitors: inspiration for clinical therapies. *Stem Cells Int* https://doi.org/10.1155/2016/6093601

Dumont NA, Wang YX, von Maltzahn J, Pasut A, Bentzinger CF, Brun CE, Rudnicki MA (2015a) Dystrophin expression in muscle stem cells regulates their polarity and asymmetric division. *Nat Med* 21: 1455 – 1463

Dumont NA, Wang YX, Rudnicki MA (2015b) Intrinsic and extrinsic mechanisms regulating satellite cell function. *Develpoment* 142: 1572 – 1581

EV-TRACK Consortium, Van Deun J, Mestdagh P, Agostinis P, Akay Ö, Anand S, Anckaert J, Martinez ZA, Baetens T, Beghein E *et al* (2017) EV-TRACK: transparent reporting and centralizing knowledge in extracellular vesicle research. *Nat Methods* 14: 228 – 232

Farup J, Madaro L, Puri PL, Mikkelsen UR (2015) Interactions between muscle stem cells, mesenchymal-derived cells and immune cells in muscle homeostasis, regeneration and disease. *Cell Death Dis* 6: e1830

Fry CS, Kirby TJ, Kosmac K, McCarthy JJ, Peterson CA (2017) Myogenic progenitor cells control extracellular matrix production by fibroblasts during skeletal muscle hypertrophy. *Cell Stem Cell* 20: 56 – 69

Gagan J, Dey BK, Layer R, Yan Z, Dutta A (2012) Notch3 and Mef2c proteins are mutually antagonistic via Mkp1 protein and miR-1/206 microRNAs in differentiating myoblasts. *J Biol Chem* 287: 40360 – 40370

Greco S, De Simone M, Colussi C, Zaccagnini G, Fasanaro P, Pescatori M, Cardani R, Perbellini R, Isaia E, Sale P *et al* (2009) Common micro-RNA signature in skeletal muscle damage and regeneration induced by Duchenne muscular dystrophy and acute ischemia. *FASEB J Off Publ Fed Am Soc Exp Biol* 23: 3335 – 3346

Guess MG, Barthel KKB, Harrison BC, Leinwand LA (2015) miR-30 family microRNAs regulate myogenic differentiation and provide negative feedback on the microRNA pathway. *PLoS ONE* 10: e0118229

Heredia JE, Mukundan L, Chen FM, Mueller AA, Deo RC, Locksley RM, Rando TA, Chawla A (2013) Type 2 innate signals stimulate fibro/adipogenic progenitors to facilitate muscle regeneration. *Cell* 153: 376 – 388

Iannotti FA, Pagano E, Guardiola O, Adinolfi S, Saccone V, Consalvi S, Piscitelli F, Gazzerro E, Busetto G, Carrella D *et al* (2018) Genetic and pharmacological regulation of the endocannabinoid CB1 receptor in Duchenne muscular dystrophy. *Nat Commun* 9: 3950

Iraci N, Leonardi T, Gessler F, Vega B, Pluchino S (2016) Focus on extracellular vesicles: physiological role and signalling properties of extracellular membrane vesicles. *Int J Mol Sci* 17: 171

Joe AWB, Yi L, Natarajan A, Le Grand F, So L, Wang J, Rudnicki MA, Rossi FMV (2010) Muscle injury activates resident fibro/adipogenic progenitors that facilitate myogenesis. *Nat Cell Biol* 12: 153 – 163

Kalluri R, LeBleu VS (2020) The biology, function, and biomedical applications of exosomes. *Science* 367: eaau6977

Kharraz Y, Guerra J, Mann CJ, Serrano AL, Muñoz-Cánoves P (2013) Macrophage plasticity and the role of inflammation in skeletal muscle repair. *Mediators Inflamm* 2013: 491497

Kitamoto T, Hanaoka K (2010) Notch3 null mutation in mice causes muscle hyperplasia by repetitive muscle regeneration. *Stem Cells* 28: 2205 – 2216

Koutsoulidou A, Mastroyiannopoulos NP, Furling D, Uney JB, Phylactou LA (2011) Expression of miR-1, miR-133a, miR-133b and miR-206 increases during development of human skeletal muscle. *BMC Dev Biol* 11: 34

Lee Y, El Andaloussi S, Wood MJA (2012) Exosomes and microvesicles: extracellular vesicles for genetic information transfer and gene therapy. *Hum Mol Genet* 21: R125 – R134

Lemos DR, Babaeijandaghi F, Low M, Chang C-K, Lee ST, Fiore D, Zhang R-H, Natarajan A, Nedospasov SA, Rossi FMV (2015) Nilotinib reduces muscle fibrosis in chronic muscle injury by promoting TNF-mediated apoptosis of fibro/adipogenic progenitors. *Nat Med* 21: 786 – 794

Liu N, Williams AH, Maxeiner JM, Bezprozvannaya S, Shelton JM, Richardson JA, Bassel-Duby R, Olson EN (2012) microRNA-206 promotes skeletal muscle regeneration and delays progression of Duchenne muscular dystrophy in mice. *J Clin Invest* 122: 2054 – 2065

Logozzi M, Angelini DF, Iessi E, Mizzoni D, Di Raimo R, Federici C, Lugini L, Borsellino G, Gentilucci A, Pierella F *et al* (2017) Increased PSA expression on prostate cancer exosomes in *in vitro* condition and in cancer patients. *Cancer Lett* 403: 318 – 329

Ma G, Wang Y, Li Y, Cui L, Zhao Y, Zhao B, Li K (2015) MiR-206, a key modulator of skeletal muscle development and disease. *Int J Biol Sci* 11: 345 – 352

Malecova B, Gatto S, Etxaniz U, Passafaro M, Cortez A, Nicoletti C, Giordani L, Torcinaro A, De Bardi M, Bicciato S *et al* (2018) Dynamics of cellular states of fibro-adipogenic progenitors during myogenesis and muscular dystrophy. *Nat Commun* 9: 3670

Mauro A (1961) Satellite cell of skeletal muscle fibers. *J Biophys Biochem Cytol* 9: 493 – 495

Minetti GC, Colussi C, Adami R, Serra C, Mozzetta C, Parente V, Fortuni S, Straino S, Sampaolesi M, Di Padova M *et al* (2006) Functional and morphological recovery of dystrophic muscles in mice treated with deacetylase inhibitors. *Nat Med* 12: 1147 – 1150

Montecalvo A, Larregina AT, Shufesky WJ, Stolz DB, Sullivan MLG, Karlsson JM, Baty CJ, Gibson GA, Erdos G, Wang Z *et al* (2012) Mechanism of transfer of functional microRNAs between mouse dendritic cells via exosomes. *Blood* 119: 756 – 766

Moyer AL, Wagner KR (2011) Regeneration versus fibrosis in skeletal muscle. *Curr Opin Rheumatol* 23: 568 – 573

Mozzetta C, Consalvi S, Saccone V, Tierney M, Diamantini A, Mitchell KJ, Marazzi G, Borsellino G, Battistini L, Sassoon D *et al* (2013) Fibroadipogenic progenitors mediate the ability of HDAC inhibitors to promote regeneration in dystrophic muscles of young, but not old Mdx mice. *EMBO Mol Med* 5: 626 – 639

Nakamura Y, Miyaki S, Ishitobi H, Matsuyama S, Nakasa T, Kamei N, Akimoto T, Higashi Y, Ochi M (2015) Mesenchymal-stem-cell-derived exosomes accelerate skeletal muscle regeneration. *FEBS Lett* 589: 1257 – 1265

Noto R, Santangelo MG, Ricagno S, Mangione MR, Levantino M, Pezzullo M, Martorana V, Cupane A, Bolognesi M, Manno M (2012) The tempered polymerization of human neuroserpin. *PLoS ONE* 7: e32444

Raposo G, Stoorvogel W (2013) Extracellular vesicles: exosomes, microvesicles, and friends. *J Cell Biol* 200: 373 – 383

Rosenberg MI, Georges SA, Asawachaicharn A, Analau E, Tapscott SJ (2006) MyoD inhibits Fstl1 and Utrn expression by inducing transcription of miR-206. *J Cell Biol* 175: 77 – 85

Saccone V, Consalvi S, Giordani L, Mozzetta C, Barozzi I, Sandoná M, Ryan T, Rojas-Muñoz A, Madaro L, Fasanaro P *et al* (2014) HDAC-regulated myomiRs control BAF60 variant exchange and direct the functional phenotype of fibro-adipogenic progenitors in dystrophic muscles. *Genes Dev* 28: 841 – 857

Sandoná M, Consalvi S, Tucciarone L, Puri PL, Saccone V (2016) HDAC inhibitors for muscular dystrophies: progress and prospects. *Expert Opin Orphan Drugs* 4: 125 – 127

Sokolova V, Ludwig A-K, Hornung S, Rotan O, Horn PA, Epple M, Giebel B (2011) Characterisation of exosomes derived from human cells by

nanoparticle tracking analysis and scanning electron microscopy. *Colloids Surf B Biointerfaces* 87: 146 – 150

Tahamtan A, Teymoori-Rad M, Nakstad B, Salimi V (2018) Anti-inflammatory microRNAs and their potential for inflammatory diseases treatment. *Front Immunol* 9: 1377

Théry C, Amigorena S, Raposo G, Clayton A (2006) Isolation and characterization of exosomes from cell culture supernatants and biological fluids. *Curr Protoc Cell Biol* 30: 3.22.1 – 3.22.29

Tidball JG (2011) Mechanisms of muscle injury, repair, and regeneration. *Compr Physiol* 1: 2029 – 2062

Tidball JG, Dorshkind K, Wehling-Henricks M (2014) Shared signaling systems in myeloid cell-mediated muscle regeneration. *Development* 141: 1184 – 1196

Trajkovic K, Hsu C, Chiantia S, Rajendran L, Wenzel D, Wieland F, Schwille P, Brügger B, Simons M (2008) Ceramide triggers budding of exosome vesicles into multivesicular endosomes. *Science* 319: 1244 – 1247

Tucciarone L, Etxaniz U, Sandoná M, Consalvi S, Puri PL, Saccone V (2018) Advanced methods to study the cross talk between fibro-adipogenic progenitors and muscle stem cells. In *Duchenne muscular dystrophy*, Bernardini C (ed) pp 231 – 256. New York, NY: Springer New York

Uezumi A, Fukada S, Yamamoto N, Takeda S, Tsuchida K (2010) Mesenchymal progenitors distinct from satellite cells contribute to ectopic fat cell formation in skeletal muscle. *Nat Cell Biol* 12: 143 – 152

Uezumi A, Ito T, Morikawa D, Shimizu N, Yoneda T, Segawa M, Yamaguchi M, Ogawa R, Matev MM, Miyagoe-Suzuki Y *et al* (2011) Fibrosis and adipogenesis originate from a common mesenchymal progenitor in skeletal muscle. *J Cell Sci* 124: 3654 – 3664

Valadi H, Ekström K, Bossios A, Sjöstrand M, Lee JJ, Lötvall JO (2007) Exosome-mediated transfer of mRNAs and microRNAs is a novel mechanism of genetic exchange between cells. *Nat Cell Biol* 9: 654 – 659

Van Deun J, Mestdagh P, Sormunen R, Cocquyt V, Vermaelen K, Vandesompele J, Bracke M, De Wever O, Hendrix A (2014) The impact of disparate isolation methods for extracellular vesicles on downstream RNA profiling. *J Extracell Vesicles* 3: https://doi.org/10.3402/jev.v3.24858

Vlassov AV, Magdaleno S, Setterquist R, Conrad R (2012) Exosomes: current knowledge of their composition, biological functions, and diagnostic and therapeutic potentials. *Biochim Biophys Acta* 1820: 940 – 948

Wang L, Zhou L, Jiang P, Lu L, Chen X, Lan H, Guttridge DC, Sun H, Wang H (2012) Loss of miR-29 in myoblasts contributes to dystrophic muscle pathogenesis. *Mol Ther J Am Soc Gene Ther* 20: 1222 – 1233

Wang XH (2013) MicroRNA in myogenesis and muscle atrophy. *Curr Opin Clin Nutr Metab Care* 16: 258 – 266

Williams AH, Valdez G, Moresi V, Qi X, McAnally J, Elliott JL, Bassel-Duby R, Sanes JR, Olson EN (2009) MicroRNA-206 delays ALS progression and promotes regeneration of neuromuscular synapses in mice. *Science* 326: 1549 – 1554

Yamamoto H, Morino K, Nishio Y, Ugi S, Yoshizaki T, Kashiwagi A, Maegawa H (2012) MicroRNA-494 regulates mitochondrial biogenesis in skeletal muscle through mitochondrial transcription factor A and Forkhead box j3. *Am J Physiol Endocrinol Metab* 303: E1419 – E1427

Yuasa K, Hagiwara Y, Ando M, Nakamura A, Takeda S, Hijikata T (2008) MicroRNA-206 is highly expressed in newly formed muscle fibers: implications regarding potential for muscle regeneration and maturation in muscular dystrophy. *Cell Struct Funct* 33: 163 – 169

Zammit PS, Golding JP, Nagata Y, Hudon V, Partridge TA, Beauchamp JR (2004) Muscle satellite cells adopt divergent fates. *J Cell Biol* 166: 347 – 357

Zhao Q, Kang Y, Wang H-Y, Guan W-J, Li X-C, Jiang L, He X-H, Pu Y-B, Han J-L, Ma Y-H *et al* (2016) Expression profiling and functional characterization of miR-192 throughout sheep skeletal muscle development. *Sci Rep* 6: 30281

